nature communications

Article

https://doi.org/10.1038/s41467-025-59462-2

HR eye & MMR eye: one-day assessment of DNA repair-defective tumors eligible for targeted therapy

Received: 4 July 2024

Accepted: 22 April 2025

Published online: 12 May 2025

Check for updates

Shinta Saito[1], Shingo Kato[2,3], Usaki Arai[1], Atsuki En[1], Jun Tsunezumi[1], Taichi Mizushima[4], Kensuke Tateishi[5] & Noritaka Adachi[1]

Homologous recombination (HR) and mismatch repair (MMR) act as guardians of the human genome, and defects in HR or MMR are causative in at least a quarter of all malignant tumors. Although these DNA repair-deficient tumors are eligible for effective targeted therapies, fully reliable diagnostic strategies based on functional assay have yet to be established, potentially limiting safe and proper application of the molecular targeted drugs. Here we show that transient transfection of artificial DNA substrates enables ultrarapid detection of HR and MMR. This finding led us to develop a diagnostic strategy that can determine the cellular HR/MMR status within one day without the need for control cells or tissues. Notably, the accuracy of this method allowed the discovery of a pathogenic *RAD51D* mutation, which was missed by existing companion diagnostic tests. Our methods, termed HR eye and MMR eye, are applicable to frozen tumor tissues and roughly predict the response to therapy. Overall, the findings presented here could pave the way for accurately assessing malignant tumors with functional defects in HR or MMR, a step forward in accelerating precision medicine.

Homologous recombination (HR) is the sole mechanism to precisely repair DNA double-strand breaks (DSBs), the most hazardous form of DNA damage. Dysfunction of HR leads to carcinogenesis in a tissue-agnostic manner, accounting for ~17% of all malignant tumors[1,2]. Approximately half of genetic mutations (and epigenetic silencing) causing HR-deficient (HRD) status occur in the *BRCA1* or *BRCA2* gene, although other HR-related genes (such as five Rad51 paralogs) are also frequently mutated in various cancers[3] (Supplementary Fig. 1a). Recent work has established that *BRCA1/2*-deficient cells and other types of HRD cells exhibit profoundly increased sensitivity to cisplatin (and other platinum based chemotherapy agents) and even more pronouncedly to poly(ADP-ribose) polymerase (PARP) inhibitor (PARPi); thus, PARPi-based therapies have emerged as successful strategies in treating breast, ovarian, pancreatic, and prostate cancers deficient in HR[4,5]. Intriguingly, chemicals that inhibit DNA polymerase theta (PolQ) are also synthetic lethal with HRD status and hold promise for effective HRD cancer treatment[6]. Despite these circumstances, current methods for validating PARPi administration in breast, pancreatic and prostate cancers have several drawbacks as these companion diagnostic assays (CDx; namely, BRACAnalysis® and FoundationOne®) are based on *BRCA1/2* sequence analysis and do not look at the functional status of HR (Supplementary Fig. 1b, c), revealing an undesirable situation that HRD cancers with no pathogenic *BRCA1/2* mutation or those with an epigenetically silenced HR-related gene are overlooked[7]. (In particular, BRACAnalysis® only inspects germline DNA, not tumor DNA, and cannot reflect the status of cancer.) Moreover, these genetic tests take

[1]Department of Life and Environmental System Science, Graduate School of Nanobioscience, Yokohama City University, Yokohama 236-0027, Japan. [2]Department of Clinical Cancer Genomics, Yokohama City University Hospital, Yokohama 236-0004, Japan. [3]Department of Gastroenterology and Hepatology, Graduate School of Medicine, Yokohama City University, Yokohama 236-0004, Japan. [4]Department of Obstetrics and Gynecology, Graduate School of Medicine, Yokohama City University, Yokohama 236-0004, Japan. [5]Department of Neurosurgery, Graduate School of Medicine, Yokohama City University, Yokohama 236-0004, Japan. e-mail: nadachi@yokohama-cu.ac.jp

a considerable amount of time (usually several weeks) for HRD/HRP determination. In ovarian cancers, >40% of which are generally supposed to be defective in HR[8], genetic testing for HRD-associated chromosomal abnormalities such as loss of heterozygosity is performed along with *BRCA1/2* sequence analysis[9]; however, it has been pointed out that this companion CDx program called myChoice® may fail to offer a genuine functional biomarker for HRD cancers, because it would take considerable time for HR-compromised cells to accumulate a sufficient number of genomic changes to be diagnosed as HRD (Supplementary Fig. 1b, c). Additionally, HR-unrelated reasons may cause similar chromosomal abnormalities[10,11]. Most importantly, those chromosomal abnormalities once arising in the genome cannot be reversed even when HR is functionally recovered, as is frequently and problematically observed in PARPi-treated tumors[12]. Several assays have been developed in an attempt to functionally investigate cellular HR status (e.g., RAD51-foci formation assay)[13], but there are many hurdles to overcome for clinical implementation, in addition to the need to improve accuracy[14].

Similar to functional defects in HR, dysfunction of mismatch repair (MMR) leads to carcinogenesis in a tissue-agnostic manner, accounting for ~17% of all malignant tumors[15,16]. MMR is a DNA repair mechanism that mends mismatched base pairs, which represent one of the most common types of chromosomal DNA damage[17]. MMR deficiency, generally called dMMR, can cause microsatellite instability (MSI) and mutation accumulation throughout the genome, resulting in MSI-High and high tumor mutation burden (TMB-High) status, respectively[18,19] (Supplementary Fig. 2a). The latter status leads to high levels of neoantigen expression, which is considered advantageous for efficient killing of dMMR cells by the immune system[15,20]. Thus, inhibiting PD-1 or PD-L1 holds an effective and promising strategy to treat dMMR tumors in a tissue-agnostic manner[15,20,21]. Another important aspect of considering MMR status in cancer therapy is that loss of MMR confers reduced sensitivity to temozolomide (TMZ, an alkylating agent), the primary drug for treating glioblastoma[22]. Because of this, long-term TMZ treatment leads to development of TMZ-resistant dMMR tumors, which show a poor prognosis[22]. Therefore, rapid diagnosis of the state of MMR in brain tumors may provide support for clinical decision on treatment strategies. Similar to the HRD circumstances stated above, diagnostic criteria for MMR status is based on "indirect" analysis, namely, either MSI analysis at several microsatellites present in the genome or immunohistochemistry (IHC) of the four major MMR proteins (i.e., MSH2, MSH6, MLH1, and PMS2) (Supplementary Fig. 2b, c). Further, these tests take ~7 days or longer and are not fully reliable, given the observations that these two dMMR tests do not necessarily give the same results with one another[23]. Additionally, MMR defects do not readily cause MSI-H status or even do not confer instability at microsatellites[24]. A proper evaluation of MMR status of tumor cells could therefore provide an invaluable tool for predicting the responsiveness of tumor patients to PD-1 as well as TMZ therapies.

Our focus in this study concerns rapid and accurate detection of cellular HR and MMR capacity. Defects in HR or MMR are responsible not only for a wide range of sporadic cancers but also for two major familial tumors, hereditary breast and ovarian cancer syndrome (HBOC) and Lynch syndrome, respectively[25,26]. As mentioned above, patients with certain types of tumors deficient in HR or MMR are eligible for PARP inhibition or PD-1 blockade therapy, respectively[5,15]. Despite these circumstances, reliable diagnostic strategies based on actual DNA repair function are yet to be established; specifically, current diagnostic approaches to these therapies rely on "indirect" analysis that only examines gene mutation or expression of limited factors and/or genomic instability, leaving epigenetic and other causes unaddressed[7,27] (Supplementary Figs. 1c and 2c).

In this study, we successfully develop cell-based functional assay methods, termed HR eye and MMR eye, that permit ultrarapid assessment of HR and MMR status in live tumor tissues even without using control cells or tissues. We propose that HR eye and MMR eye offer additional tools for assessment and validation of HRD and dMMR tumors and could contribute to acceleration of precision medicine.

Results

Rapid detection of cellular HR activity via transient DNA transfection

To overcome the aforementioned challenges in evaluating the relevant DNA repair defects, we first sought to develop a cell-based assay system to rapidly detect cellular HR activity. For this purpose, we designed and generated a DNA construct, pCMV-GapNluc-iNluc, which contains two imperfect NanoLuc (Nluc) gene fragments *GapNluc* and *iNluc*, as depicted in Fig. 1a and Supplementary Fig. 3a, b. We assumed that this construct, termed "HR-Nluc-v1", would allow for Nluc expression after transfection when HR occurs between the imperfect fragments to generate an intact *Nluc* gene. We also generated a DNA construct, pCMV-5'Nluc-3'Nluc, comprising *5'Nluc* and *3'Nluc* (which lack a 3' or 5' side of the *Nluc* gene, respectively); from this construct (SSA-Nluc-v1), Nluc is only expressed when a recombination reaction occurs between *5'Nluc* and *3'Nluc* (Fig. 1a). This type of recombination, generally called single-strand annealing (SSA), is mechanistically and genetically distinct from HR[28]. We transfected each construct, HR-Nluc-v1 or SSA-Nluc-v1, into six different human cell lines to monitor luciferase activity. As shown in Fig. 1b and Supplementary Fig. 3c, luciferase activity was detected 2 h after HR-Nluc-v1 transfection and reached a plateau at 8 h in all cell lines tested, indicating the expected occurrence of HR to mend the gap in the *GapNluc* fragment. Transfection of SSA-Nluc-v1 (Fig. 1b) yielded similar results, and Nluc expression was detected as early as 1 h after transfection and the expression levels were consistently higher than that of HR-Nluc-v1, suggesting a quick occurrence of SSA compared to the HR reaction (Fig. 1c and Supplementary Fig. 3c, d). Interestingly, the frequency of SSA is comparable between different cell lines and consistently higher than that of HR, which varies among the cell lines, with Nalm-6 being quite low, an observation consistent with previous reports[29,30] (Fig. 1c and Supplementary Fig. 3d). It is important to mention that we performed similar experiments using GFP-based constructs and obtained essentially the same results; however, a longer time was required for detecting recombination-dependent gene expression and the assay sensitivity was significantly low compared with Nluc-based constructs (Supplementary Fig. 4). We also used a secretion-type Nluc and a proteasome-sensitive Nluc with reduced protein stability, but these constructs were ineffective in enhancing sensitivity for detecting extrachromosomal HR (Supplementary Fig. 3e, f).

Notably, we found that extrachromosomal HR and SSA (hereafter ecHR and ecSSA, respectively) reactions are mechanistically similar to chromosomal HR and SSA reactions, as evidenced by the following observations: (1) gene knockdown of Rad51, which is absolutely required for HR[31], markedly reduced ecHR and not ecSSA (Fig. 1d); (2) BRCA1/BRCA2-deficient cells exhibited lower ecHR activity than the proficient cells (Fig. 1e); (3) Knockout of Rad52, a key factor in SSA[32], reduced ecSSA and not ecHR (Supplementary Fig. 5a, c); (4) Gene-knockout cell lines with reduced HR activity (e.g., *RAD54*$^{-/-}$)[33] displayed reduced ecHR and increased ecSSA, whereas cells deficient in NHEJ[34] showed increased levels of ecHR and ecSSA (Supplementary Fig. 5a, c). All these observations were essentially the same as those that have been obtained from chromosomal recombination assays using DR-GFP and SA-GFP reporter constructs[35,36] (Supplementary Fig. 5a–d). We note that, for correctly measuring ecHR, the direction of *iNuc* relative to *GapNluc*, but not the distance between *GapNluc* and *iNluc* in the construct, is significant (Supplementary Fig. 6a–f; HR-Nluc-v1.1, HR-Nluc-v1.2, HR-Nluc-v1.3). Intriguingly, for ecHR to take place, *GapNluc* and *iNluc* can be placed on separate DNA molecules, especially when an *iNluc*-carrying DNA is in a circular form (Fig. 1f; pCMV-GapNluc +

https://doi.org/10.1038/s41467-025-59462-2

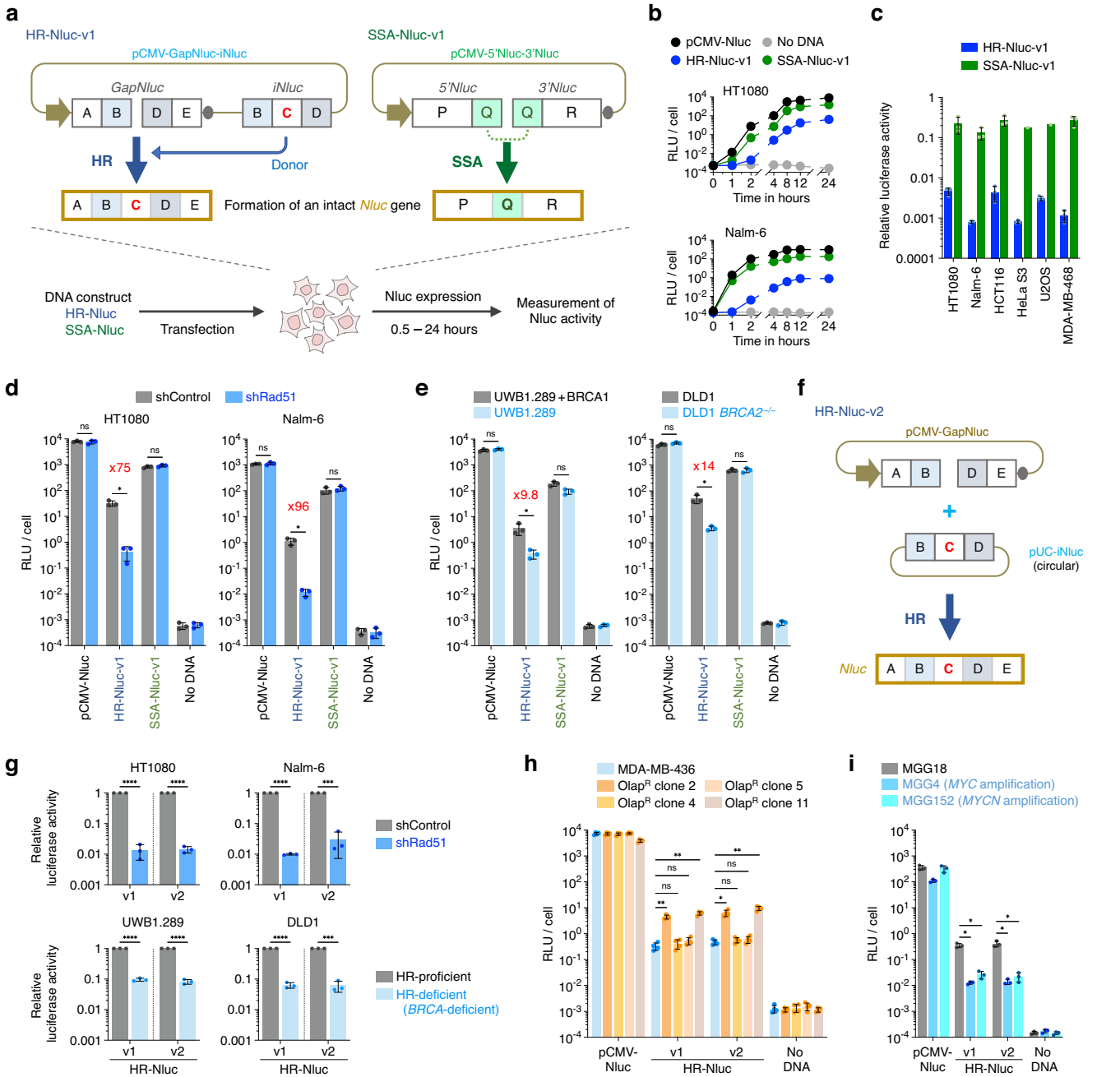

Fig. 1 | Rapid detection of cellular HR and SSA activity by transient DNA transfection. a Schematic of *Nluc*-based DNA constructs to detect HR (HR-Nluc-v1) and SSA (SSA-Nluc-v1). Horizontal arrow, CMV promoter; gray oval, polyA signal. **b** Monitoring of luciferase activity in human HT1080 and Nalm-6 cell lines following transfection. **c** Comparison of HR and SSA activity in 6 different human cell lines. Luciferase activity was measured 24 h after transfection, and relative luciferase activity (pCMV-Nluc was taken as 1) was calculated from the data shown in **b** and Supplementary Fig. 3c. Data shown are the mean ± s.d. of three independent experiments, except for SSA analysis using HeLa S3 and U2OS. **d** Impact of Rad51 knockdown on extrachromosomal HR and SSA in HT1080 and Nalm-6 cells. Data shown are the mean ± s.d. of three independent experiments. **e** Impact of BRCA1/BRCA2 deficiency on extrachromosomal HR and SSA. Data shown are the mean ± s.d. of three independent experiments. **f** Schematic of HR-Nluc-v2. Note that imperfect *Nluc* fragments are placed on separate DNA molecules, with *iNluc*-carrying DNA in a circular form so that HR dominates over SSA (see Supplementary Fig. 5f). **g** Impact of HR deficiency on extrachromosomal HR of HR-Nluc-v1 and HR-Nluc-v2. The relative luciferase activity (HR-deficient vs HR-proficient) is shown in (**d** and **e**). Symbols are as in (**d** and **e**). Data shown are the mean ± s.d. of three independent experiments. **h** Analysis of HR status of MDA-MB-436-derived olaparib-resistant clones. Data shown are the mean ± s.d. of four independent experiments. Note that shown are the results of 4 out of 11 olaparib-resistant clones, and the results of all the resistant clones are shown in Supplementary Fig. 7b. **i** Analysis of HR status of Myc/Mycn-overexpressing cells harboring *MYC/MYCN* gene amplification. Data shown are the mean ± s.d. of three independent experiments. Statistical significance was determined by two-sided Student's t-test (**d**, **e**, and **g**), or by one-way ANOVA with Dunnett's multiple comparisons (**h** and **i**). $^{*}P < 0.05$; $^{**}P < 0.01$; $^{***}P < 0.001$; $^{****}P < 0.0001$; ns, not significant. Source data are provided as a Source Data file.

pUC-iNluc), while SSA predominantly occurred when *iNluc* was supplied as a short linear DNA (Supplementary Fig. 5e, f). The "pCMV-GapNluc + pUC-iNluc" system, termed "HR-Nluc-v2", was found to be as reliable as HR-Nluc-v1 to monitor ecHR and showed similar genetic requirements for the ecHR reaction (Fig. 1g and Supplementary Figs. 5a–f and 6c–g).

Importantly, HR-Nluc-v1 and HR-Nluc-v2 are both capable of inquiring into the state of HR of *BRCA*-deficient cells that have acquired

PARPi resistance. We isolated 11 olaparib-resistant clones from the *BRCA1*-deficient breast cancer cell line MDA-MB-436[37] and confirmed that two of these clones displayed a significant (~13 to 20-fold) increase in ecHR activity compared with parental cells (Fig. 1h and Supplementary Fig. 7a, b). These HR-restored cells led to cell death upon transfection of a modified HR-Nluc construct that allows for *DT-A* expression in an ecHR-dependent manner, confirming that the observed PARPi resistance in these clones had been acquired via an HR-restoring genetic change(s) (Supplementary Fig. 7c, d). We observed a similar ecHR-mediated cell killing in *RAD54*$^{-/-}$*RAD54B*$^{-/-}$ cells, and not in HR-proficient cells (Supplementary Fig. 7e). The utility of HR-Nluc-v1 and HR-Nluc-v2 was further highlighted by our experiments using the brain tumor cell lines MGG4 and MGG152. These cells are hypersensitive to PARPi because of Myc/Mycn overexpression[38] and our results indeed revealed a significantly lower HR activity in these cells than in the control cell line MGG18[38] (Fig. 1i). Together, these results indicate that the HR-Nluc system allows for rapid assessment of HRD status, not just for *BRCA*-deficient cells but also for cells with reduced HR activity caused by other factors.

Rapid detection of MMR activity using ecSSA-detecting DNA constructs

We next sought to develop a cell-based assay method that can rapidly assess the MMR status. For this purpose, we employed the SSA-Nluc-v1 system that allows efficient monitoring of ecSSA. Since MMR proteins are known to suppress SSA in lower eukaryotes when sequence homology is imperfect[39], we reasoned that ecSSA between homeologous sequences would be enhanced in MMR-deficient (dMMR) cells. Upon transfection of SSA-Nluc-v1 derivatives harboring mismatched bases in a recombination substrate (i.e., a 5′-portion of *3′Nluc*) (Fig. 2a and Supplementary Fig. 8a, b), dMMR cells displayed higher ecSSA activity than did MMR-proficient (pMMR) cells, depending on the increase in sequence divergence between recombination substrates (Supplementary Fig. 9a), consistent with heteroduplex rejection exerted by MMR proteins[30,39–41]. However, the stimulatory effect of dMMR was only evident in Nalm-6 and not in other cell lines (Fig. 2b and Supplementary Fig. 9b–d). As an attempt to increase the impact of dMMR on SSA enhancement, we designed and tested SSA-Nluc-v2 and SSA-Nluc-v3, which both comprise pCMV-GapNluc plus an *iNuc* fragment(s), requiring more than one SSA reactions to generate the intact *Nluc* gene (Fig. 2a and Supplementary Fig. 8c–e). These constructs, when harboring sequence divergence, were effective in improving the sensitivity to assess MMR status (Fig. 2b, c), although a sharp drop in luciferase activity was observed with SSA-Nluc-v3 constructs with extensive sequence divergence (Fig. 2b, c and Supplementary Fig. 9b–d). Thus, dMMR-associated SSA enhancement was clearly observed with the SSA-Nluc-v2 system, as was further confirmed by gene-knockdown experiments using *MSH2*, *MSH6*, *MLH1* and *PMS2* siRNAs (Fig. 2d).

Assessment of HRD and dMMR status without control cells

Our findings described above demonstrate that transient transfection of designed DNA constructs enables rapid determination of cellular HR and MMR capacity when control cells are available; more specifically, when HR-Nluc constructs were transfected, HR-proficient (HRP) cells displayed greater Nluc activity than HRD cells, while SSA-Nluc constructs with sequence divergence conferred higher levels of Nluc expression in dMMR cells than in pMMR cells. To implement these methods as therapeutic biomarkers, however, DNA repair status must be presented as absolute scores, ideally with bimodal distribution, because control cells (i.e., non-tumor samples) are not always available from the patient. We therefore carefully and thoroughly compared all of the above data derived from solid tumor cell lines by calculating the ratio of Nluc activity of each DNA repair-detecting construct to that of an independently transfected control vector (typically, pCMV-Nluc).

Intriguingly, the HR-Nluc-v1 / pCMV-Nluc ratio of all HRD solid tumor cell lines was consistently lower than that of otherwise isogenic HRP cell lines (including the HR-restored MDA-MB-436 cell line) (Supplementary Fig. 10a). This bimodal distribution was similarly seen in HR-Nluc-v1.2 and HR-Nluc-v2. We verified the bimodal distribution of Nluc activity from HRD/HRP populations by employing 13 additional solid tumor cell lines, where isogenic controls were unavailable (Supplementary Fig. 10b). As shown in Supplementary Fig. 10c, this analysis revealed that the HR-Nluc-v1 / pCMV-Nluc ratio was consistently lower than 0.00047 in all HRD cell lines and higher than 0.00074 in all HRP cell lines. Similarly, the HR-Nluc-v2 / pCMV-Nluc ratio was consistently lower than 0.00037 in all HRD cell lines and higher than 0.00089 in all HRP cell lines (Supplementary Fig. 10c). Such bimodal distribution was also seen in HR-Nluc-v1.2, but never observed with the GFP-based constructs (Supplementary Fig. 10c, f), implying the superiority of Nluc as a reporter protein. Based on these findings, we termed our HR-Nluc-based technology "HR eye_1 (or _2)" or "Accurate Direct Assay for Cellular HRD Index (ADACHI) method" and defined "ADACHI Score" as the formula "[pCMV-Nluc] / 1,351 x [HR-Nluc-v1]" or "[pCMV-Nluc] / 1,124 x [HR-Nluc-v2]", finally defining HRD status as an ADACHI Score value of >1 (Fig. 3a and Supplementary Fig. 10d, e). As shown in Fig. 3b, we confirmed the perfect bimodal distribution of ADACHI Score values calculated from HRP and HRD cell populations.

We next examined the relationship between HR eye-based ADACHI Score and cellular sensitivity to PARPi (olaparib, niraparib and talazoparib), PolQi (ART558, RP-6685 and novobiocin), and other drugs that cause HR repair-requiring DNA damage (cisplatin and camptothecin)[42]. We found that not only can ADACHI Score assess HRD status but also may be capable of predicting drug efficacy. Clearly, cells showing >1 Score values were highly sensitive to PARPi and PolQi compared to those with <1 Score values, as was true for both HR eye_1 and _2 (Fig. 3c and Supplementary Fig. 11). This may not be surprising, given the fact that HRD cells exhibit increased sensitivities to these drugs[4–6]. Strikingly, however, ADACHI Score displayed a substantial linear correlation to cellular sensitivity to PARPi and PolQi (Fig. 3d and Supplementary Fig. 11). In particular, PARPi sensitivity was very well correlated with ADACHI Score, providing a fascinating prediction that cells with high ADACHI Score values will proportionally display high sensitivity to PARPi. Likewise, ADACHI Score showed a good linear correlation with sensitivity to cisplatin and weakly to camptothecin, but not to irrelevant genotoxic agents (etoposide and TMZ; Fig. 3d and Supplementary Fig. 11). It is interesting to mention that, in addition to HR-restored *BRCA1*-deficient cells, MGG4 and MGG152, which are hypersensitive to PARPi because of Myc/Mycn overexpression[38], also showed > 1 ADACHI Score values (Fig. 3b), confirming the reliability of HR eye as a therapeutic biomarker for drug efficacy prediction as well as HRD determination.

We next wished to establish a reliable biomarker for MMR-defective status as well. For this purpose, we calculated and compared the ratio of Nluc activity obtained from homeologous SSA-Nluc systems (in which the recombination substrates have sequence divergence) to homologous ones. This comprehensive analysis, as shown in Supplementary Fig. 12a–c, led us to find that SSA-Nluc-v2, but not v1 or v3, does offer reliable values for assessing the state of MMR. Specifically, the ratio of 90% to 100% homology construct of SSA-Nluc-v2 was consistently lower in pMMR cell lines than in dMMR counterparts (including TMZ-resistant MGG152 cells, which had lost Msh2/Msh6 expression due to *MSH6* promoter methylation[43]) (Supplementary Fig. 12b). The bimodal distribution of Nluc activity from dMMR/pMMR populations was further confirmed by employing 12 additional tumor cell lines (Supplementary Fig. 12d). This analysis again revealed that the SSA-Nluc-v2-based system is indeed reliable to determine the MMR

https://doi.org/10.1038/s41467-025-59462-2

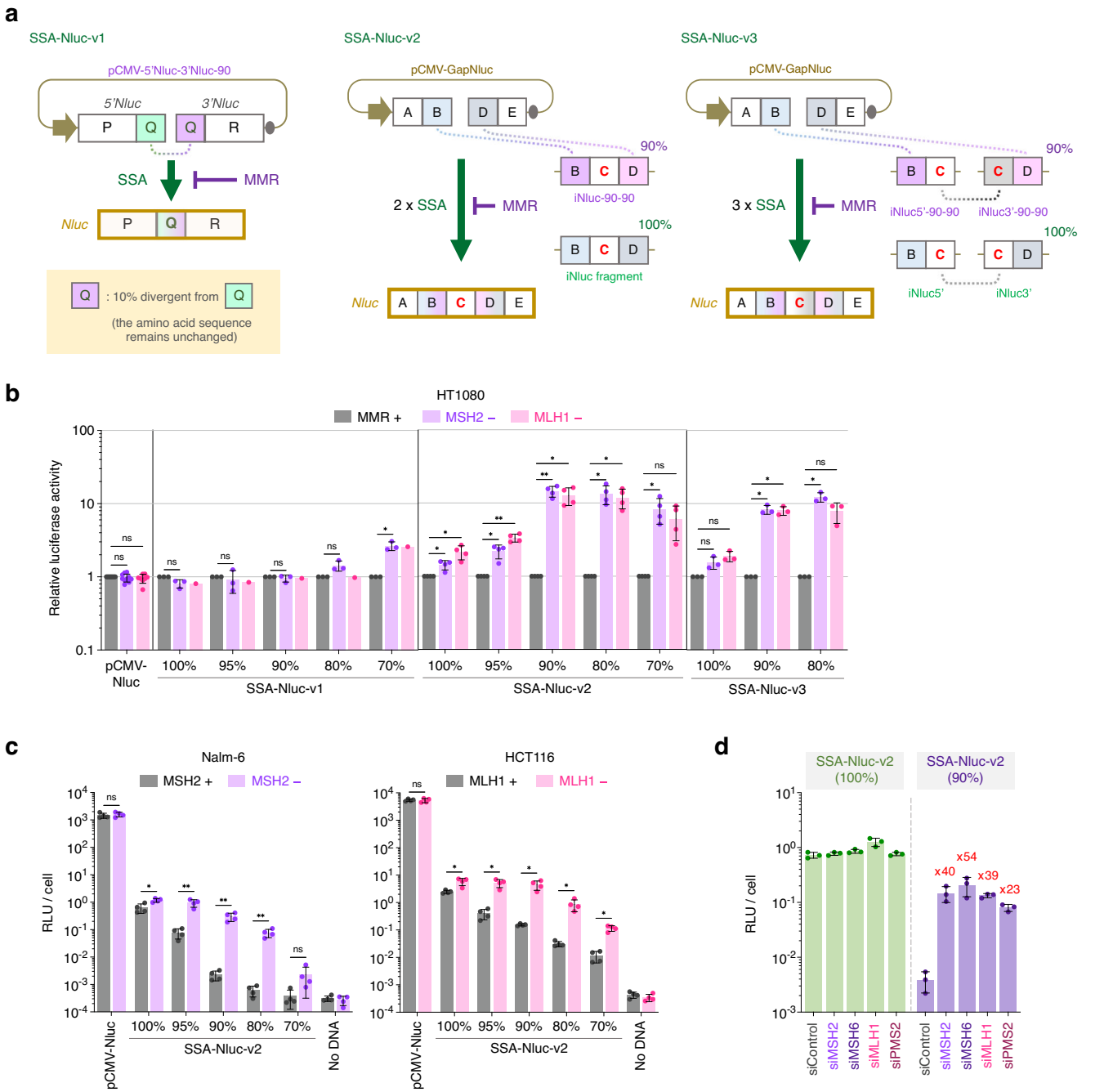

Fig. 2 | Rapid determination of MMR status using modified SSA-Nluc constructs. a Schematic of SSA-Nluc constructs with mutated recombination substrates. SSA-Nluc-v2 and v3, unlike SSA-Nluc-v1, requires more than one SSA reactions for Nluc expression. For simplicity, only 100% and 90% homology constructs are shown. **b** Impact of sequence divergence on extrachromosomal SSA in HT1080. Luciferase activity was measured 24 h after transfection. Shown is the relative luciferase activity (MSH2– or MLH1– vs MMR +), based on the data shown in Supplementary Fig. 9b. Data shown are the mean ± s.d. of three (SSA-Nluc-v1 and v3) or four (SSA-Nluc-v2) independent experiments. **c** Impact of MMR loss on extrachromosomal SSA using SSA-Nluc-v2. Luciferase activity was measured 24 h after transfection. Data shown are the mean ± s.d. of four (Nalm-6) or three (HCT116) independent experiments. **d** Impact of MMR-gene knockdown on extrachromosomal SSA in *MSH2*-corrected Nalm-6 cells. The 100% and 90% homology constructs of SSA-Nluc-v2 were used for experiments. Data shown are the mean ± s.d. of three independent experiments. Statistical significance was determined by one-way ANOVA with Dunnett's multiple comparisons (**b**), or by two-sided Student's t-test (**c**). $^{*}P < 0.05$; $^{**}P < 0.01$; ns, not significant. Source data are provided as a Source Data file.

status even without using near-isogenic control cells. Specifically, the ratio of 90% / 100% homology construct is consistently higher than 0.256 in all dMMR cell lines and lower than 0.081 in all pMMR cell lines (Supplementary Fig. 12e). Based on these findings, we termed our SSA-Nluc-v2-based technology "MMR eye" and defined "dMMR Score" as the formula "1/0.081 x [SSA-Nluc-v2 (90%)] / [SSA-Nluc-v2 (100%)]", finally defining dMMR status as a dMMR Score value of >1 (Fig. 4a and Supplementary Fig. 12f, g). As shown in Fig. 4b, we confirmed a perfect bimodal distribution of dMMR Score values calculated from pMMR and dMMR cell populations. Intriguingly, cellular sensitivity to TMZ, to which dMMR cells showed an increased resistance[43], was positively correlated with dMMR Score (Fig. 4c, d and Supplementary Fig. 13), confirming the clinical utility of dMMR Score as a therapeutic biomarker.

https://doi.org/10.1038/s41467-025-59462-2

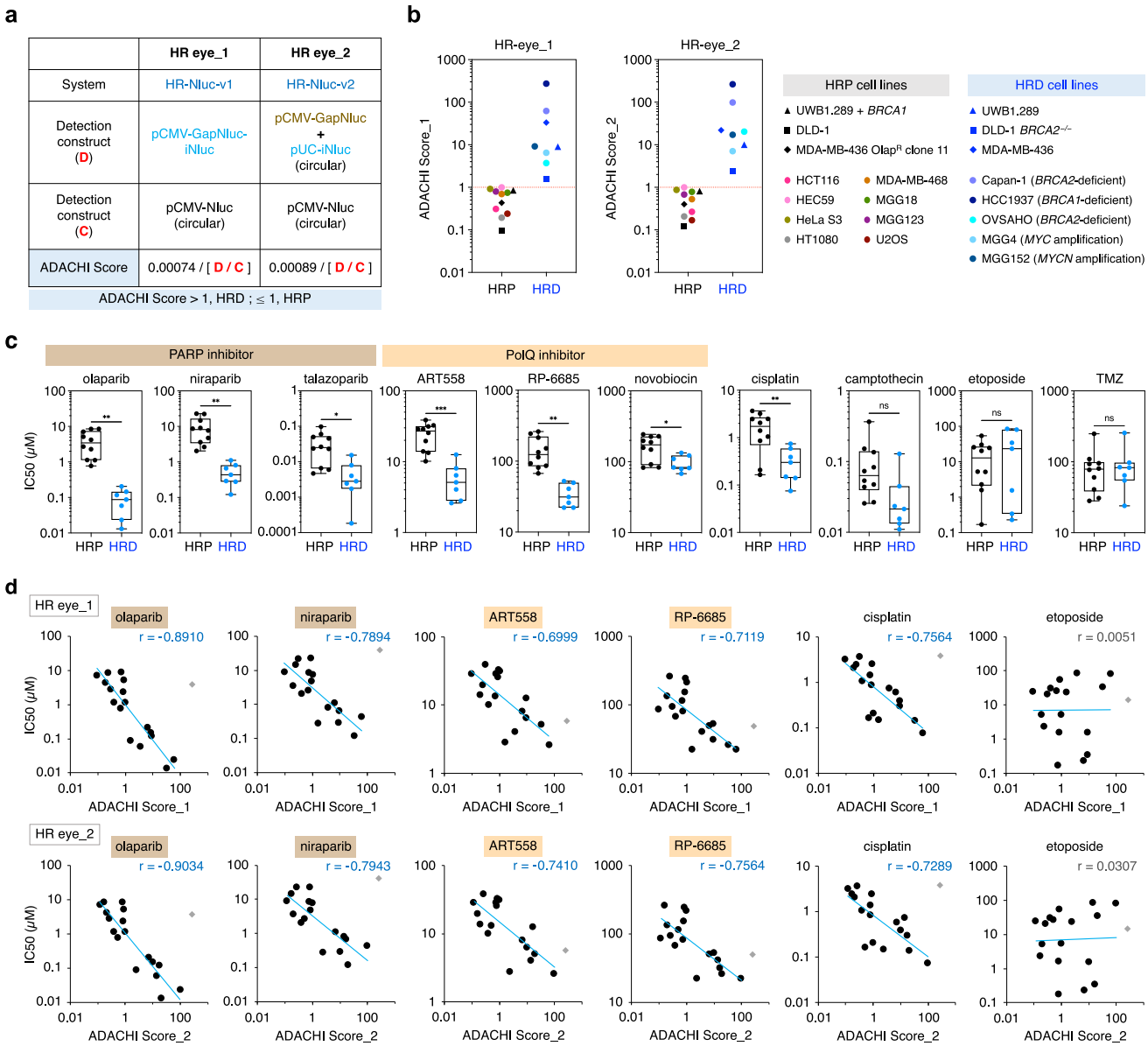

Fig. 3 | Development of a scoring system to define HR deficiency. a Schematic of HR eye. Definition of ADACHI Score_1 and ADACHI Score_2 as a biomarker for HRD determination is also indicated. **b** ADACHI Score values of HRP and HRD cell lines as determined by HR eye_1 and HR eye_2. ADACHI Score values were calculated from the data shown in Supplementary Fig. 10c, and the mean values of four (MDA-MB-436) or three (other cell lines) independent experiments are indicated. **c** Comparison of HR status and drug sensitivity. Seventeen different cells were determined for HR status using HR eye. Drugs used were PARP inhibitors (olaparib, niraparib and talazoparib), PolQ inhibitors (ART558, RP-6685 and novobiocin), cisplatin, camptothecin, etoposide, and TMZ. Note that TMZ was used along with 5 μM O^6-benzylguanine (see Methods). The IC50 value for each drug was calculated based on the data shown in Supplementary Fig. 11a, and the mean values of three independent experiments are indicated. Line in the box corresponds to the median; lower and upper edges of the box indicating the first and third quartiles; whiskers extend to minimum and maximum values. **d** Correlation between ADACHI Score and drug sensitivity. Drugs used were PARP inhibitors (olaparib and niraparib), PolQ inhibitors (ART558 and RP-6685) and cisplatin. Light blue lines represent results of linear regression analysis. r, Pearson correlation coefficient. Note that the data for HCC1937 (gray diamond) were omitted from the analysis, as this HRD cell line has been shown to be PARPi resistant due to lack of FAM35A expression[95]. Etoposide served as a control drug. Statistical significance in **c** was determined by two-sided Student's t-test. *$P < 0.05$; **$P < 0.01$; ***$P < 0.001$; ns, not significant. Source data are provided as a Source Data file.

HR eye and MMR eye are implementable to tumor tissues from human patients as well as CDX and PDX mouse models

To validate the practical usefulness of HR eye and MMR eye for solid tumor tissues, we employed many different CDX and PDX mouse models (Fig. 5a). The CDX models were established by subcutaneous or orthotopic transplantation of 9 different solid tumor cell lines, and the PDX models were established by orthotopic transplantation of 6 different brain tumor-derived cell lines. As expected, HRD and dMMR status were correctly assessed in all tumor tissues originated from DNA repair-deficient cells, while HRP and pMMR tissues were correctly judged to be repair-proficient (Fig. 5b, c). In all cases, assay results were successfully obtained within one day (~25 h after tissue dissociation). Here again, HR-Nluc-v1 and HR-Nluc-v2 were both capable of assessing the HRD status of cells from live tissues. For dMMR determination, SSA-Nluc-v2 alone was competent in assessing dMMR status (Fig. 5b, c). We note that the assay results of repair-deficient tumor tissues were somewhat lower than that of cultured cells, perhaps reflecting contamination of repair-proficient murine cells into the tumor tissue (Fig. 5b). In this regard, it is worth mentioning that we actually examined the impact of HRP/pMMR cell contamination on

https://doi.org/10.1038/s41467-025-59462-2

a

	MMR eye
System	SSA-Nluc-v2
Detection construct (D)	pCMV-GapNluc + iNluc-90-90
Detection construct (C)	pCMV-GapNluc + iNluc fragment
dMMR Score	[1 / 0.081] x [D / C]
> 1, dMMR ; ≤ 1, pMMR	

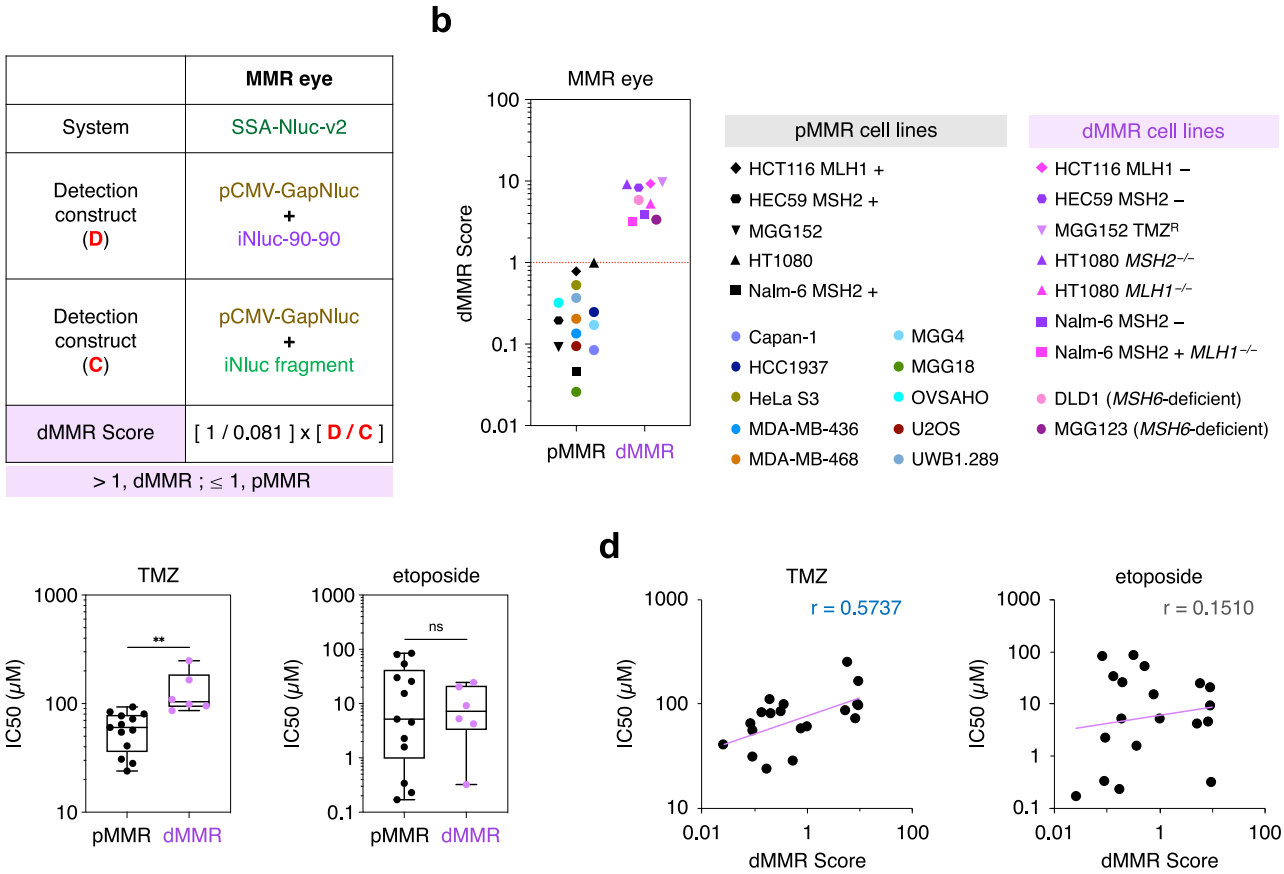

Fig. 4 | Development of a scoring system to define MMR deficiency. a Schematic of MMR eye. Definition of dMMR Score as a biomarker for dMMR determination is also indicated. **b** dMMR Score values of pMMR and dMMR cell lines as determined by MMR eye. The dMMR Score values were calculated from the data shown in Supplementary Fig. 12e, and the mean values of four (HT1080, Nalm-6, and HCT116) or three (other cell lines) independent experiments are indicated. **c** Comparison of MMR status and drug sensitivity. Nineteen different cell lines were determined for MMR status using MMR eye. The IC50 values for TMZ and etoposide were calculated based on the data shown in Supplementary Fig. 13a, and the mean values of three independent experiments are indicated. Line in the box corresponds to median; lower and upper edges of the box indicating the first and third quartiles; whiskers extend to minimum and maximum values. **d** Correlation between dMMR Score and TMZ sensitivity. Light purple lines represent results of linear regression analysis. r, Pearson correlation coefficient. Etoposide served as a control drug. Statistical significance in **c** was determined by two-sided Student's t-test. **P < 0.01; ns, not significant. Source data are provided as a Source Data file.

HRD/dMMR determination of HRD/dMMR cells using different cell lines and showed that, for correctly assessing HRD status, HR eye permits ~50% inclusion of HRP cells in the cell population (Fig. 5d and Supplementary Fig. 14a, b), while MMR eye permits as high as 70% contamination of pMMR cells for correct dMMR determination (Fig. 5e and Supplementary Fig. 14c). Our findings obtained from mouse model experiments and the experiments using intentionally mixed cell lines suggest that, despite the definition of >1 ADACHI/dMMR Score values to be HRD/dMMR, Score values lower than 1 could still represent HRD/dMMR status. This would particularly be true for clinical specimens with low tumor cellularity or substantial intratumor heterogeneity[44,45] (see Discussion). We underline that the above-described mouse model experiments were performed using a variety of solid tumor cell lines that had been established from tissues where DNA repair deficiency is frequent (e.g., breast, colorectal, pancreatic, endometrial, and TMZ-treated brain tumors)[1,2,15,16], implying that the HR eye and MMR eye methods are indeed applicable to these clinically important solid tumors.

We next set out to apply our methods to tumor tissues from human patients with brain tumors (Fig. 6a and Supplementary Fig. 15a). In all cases analyzed, HR eye and MMR eye results were successfully obtained (Fig. 6b and Supplementary Fig. 15b), despite the obvious difference in transfection efficiency between different samples (i.e., RLU/cell values of pCMV-Nluc ranged from ~35 to >500; Supplementary Fig. 15c). As shown in Fig. 6b and Supplementary Fig. 15b, all tissue samples tested showed <1 ADACHI Score values and were assessed as HRP, consistent with the rarity of HRD brain tumors[2,38]. Although cases of dMMR were also infrequent, tumors from patients who underwent long-term TMZ chemotherapy exhibited high dMMR Score values (10.78 for BT#1 R, 1.48 for BT#20 R, and 4.67 for BT#21 R) (Fig. 6b and Supplementary Fig. 15b). Sequence analysis revealed that BT#20 R and BT#20RR had pathogenic mutations in two MMR genes, namely *MLH1* (p.Y561fs*7) and *MSH6* (p.F1088fs*2), supporting high accuracy of dMMR determination by our method. Another sample, BT#1 R, had no mutation in the four MMR genes and did not display MSI-High phenotype, but apparently lacked expression of MLH1 and PMS2 proteins (Fig. 6c), providing decisive evidence for this tumor being dMMR. Thus, our results indicate that the MMR status of recurrent tumors resulting from long-term TMZ exposure can be easily and accurately monitored by the MMR eye method, even when any MMR gene mutation or MSI-High phenotype is not observed.

To further confirm the utility value of HR eye in clinical settings, we finally examined the HR status of 37 tissue samples from ovarian cancer patients (Fig. 6d and Supplementary Fig. 16a–d). Additionally, where possible, we compared the results of HR eye with that of existing companion diagnostic tests approved for ovarian cancer (see Supplementary Fig. 1b). Again, despite the considerable difference in transfection efficiency between tumor samples (i.e., RLU/cell values of

https://doi.org/10.1038/s41467-025-59462-2

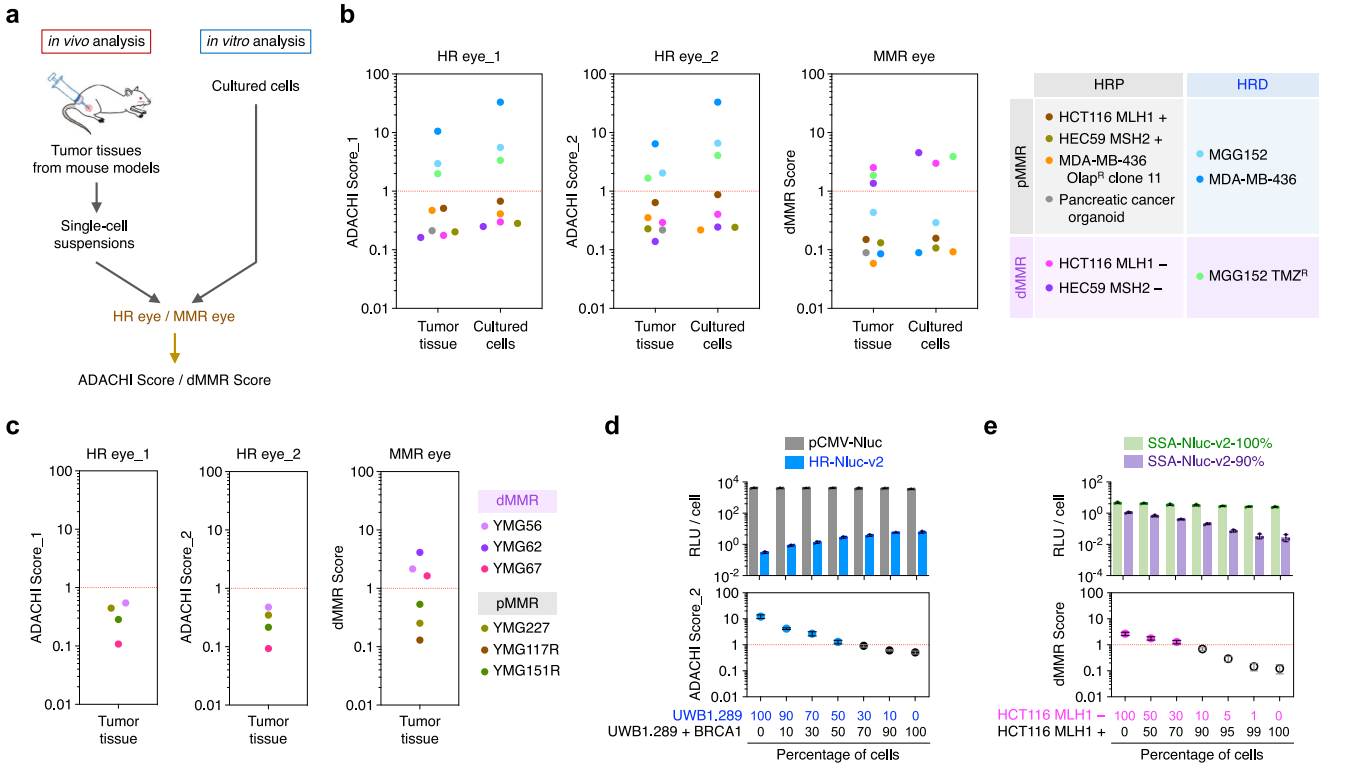

Fig. 5 | Validation of HR eye/MMR eye-based Score values using tumor tissues from mouse models. a Schematic representation of analysis using tumor tissues from CDX and PDX mouse models. **b** ADACHI Score and dMMR Score values determined using tumor tissues from CDX models. For comparison, data from in vitro analysis are also shown ("Cultured cells"). Summarized on the right is the HR and MMR status of the cell lines used. **c** ADACHI Score and dMMR Score values determined using tumor tissues from PDX models. Note that YMG56 exhibits TMB-High status (75 mut/Mb), and YMG62 and YMG67 harbor an *MSH6* gene mutation (p.L1291N or p.E993del, respectively) (see Methods). **d** Impact of cell contamination on HR eye_2 test results. pCMV-Nluc or HR-Nluc-v2 was transfected into UWB1.289 (*BRCA1*-corrected and uncorrected) cell mixture. Luciferase activity was measured 24 h after transfection. Data shown are the mean ± s.d. of three independent experiments. **e** Impact of cell contamination on MMR eye test results. SSA-Nluc-v2 (100% or 90% homology construct) was transfected into HCT116 (*MLH1*-corrected and uncorrected) cell mixture. Luciferase activity was measured 24 h after transfection. Data shown are the mean ± s.d. of three independent experiments. Source data are provided as a Source Data file.

pCMV-Nluc ranged from ~1 to 2000) (Supplementary Fig. 16d), HR eye results were successfully obtained using frozen as well as refrigerated samples (Fig. 6d and Supplementary Fig. 16c–e). We note that OC#1 and OC#12 showed substantially low transfection efficiency (i.e., RLU/cell value of pCMV-Nluc was <2), which we speculate is presumably due to the low number of viable cells, as these tumors were treated with standard chemotherapy before surgery (see Discussion). Surprisingly, frozen tissue samples were all assay-competent for one week after surgery, and as many as ~80% of samples re-examined were tolerant to two week-storage at −80 °C (summarized in Supplementary Fig. 16e). Refrigerated samples preserved at 4 °C seemed susceptible to long-term storage compared with frozen samples, and yet they all remained assay-competent for 3 days after surgery (Supplementary Fig. 16e).

As expected, HR eye results obtained from high-grade serous carcinoma (HGSC) indicated that 9 out of 20 cases were HRD, while the other types of ovarian cancer showed lower incidence of HRD (3 out of 17) (Supplementary Fig. 16c), an observation consistent with the existing literature that HRD is highly frequent in HGSC[8]. We next compared the results of HR eye with that of myChoice®, a companion diagnostic test approved for ovarian cancer[46]. This diagnostic is based on two criteria for HRD determination, a pathogenic *BRCA1/2* gene mutation and/or a high (≥ 42) GI score (in which GI stands for genome instability that is algorithmically determined by sequence analysis based on the extent of three types of chromosomal abnormalities, LOH, TAI, and LST)[9] (see Supplementary Fig. 1). Notably, the above-described HR eye results showed a good correlation with the test results of myChoice®: The agreement between HR eye_1 and myChoice® was 64% (9/14), and between HR eye_2 and myChoice® was 90% (9/10) (Fig. 6e and Supplementary Fig. 16c). Three samples diagnosed as HRD in myChoice® (OC#24, OC#28, OC#29) were reasonably judged as HRD in HR eye_2, but not in HR eye_1, where the ADACHI Score values were somewhat lower than 1 (Fig. 6e). This implies, provided that the results of HR eye_2 and myChoice® are both correct, that HR eye_1 may be somewhat less reliable than HR eye_2 perhaps due to its vulnerability to low tumor content (i.e., noncancerous cell contamination) and/or tumor heterogeneity (see Discussion). Indeed, all tumor tissues harboring a pathogenic *BRCA1/2* mutation were correctly judged to be HRD in HR eye_v2 (Fig. 6e).

Interestingly, tissue samples OC#4 M and OC#10 diagnosed as HRP in myChoice® were determined to be HRD in our HR eye test (Fig. 6e). OC#10 had no *BRCA1/2* mutations and the actual HR status of this tumor is currently unclear, even given accuracy of the HR eye assay. On the other hand, sequence analysis revealed that OC#4 M harbors a variant of uncertain significance (VUS) mutation (c.196 G > A; p.V66M) in *RAD51D*, a gene encoding one of the five Rad51 paralogs. Although this mutation has been recognized to be benign, not cancerous[47,48], and the FoundationOne® test also judged this tumor as HRP, a recent report revealed that Rad51D Val66 is important for XRCC2 binding[49]. Since Rad51 paralogs play as critical a role as BRCA1/2 in HR[50–52], we reasoned that the p.V66M mutation would significantly affect HR. This was indeed the case. We knocked out the *RAD51D* gene in HT1080 cells (Fig. 6f), and confirmed that the gene knockout led to a significant decrease in HR activity (Fig. 6g) and a concomitant increase in sensitivity to olaparib (PARPi), ART558 (PolQi) and cisplatin (Fig. 6h).

https://doi.org/10.1038/s41467-025-59462-2

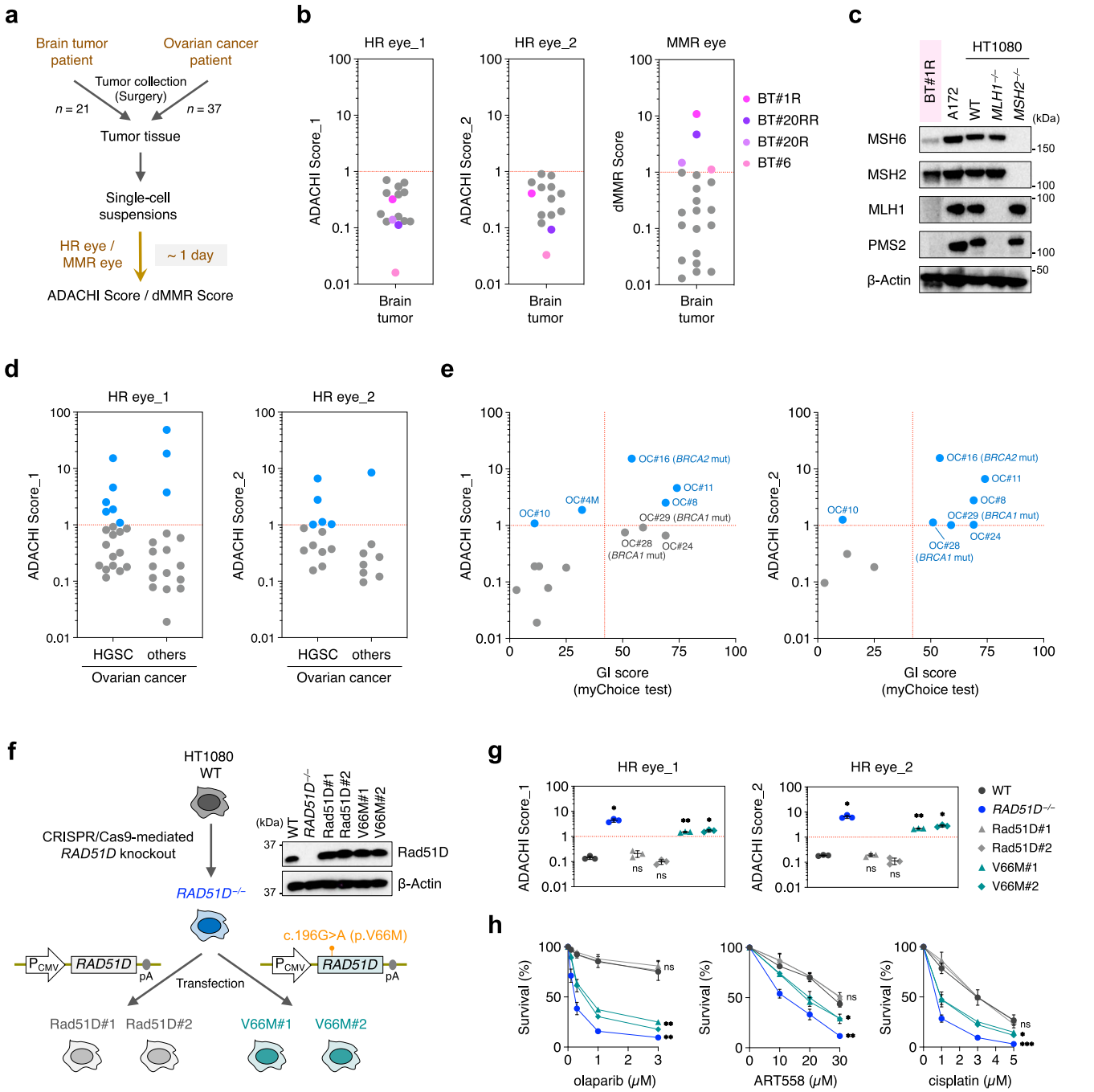

Fig. 6 | Validation of HR eye/MMR eye-based Score values using patient biopsies. a Schematic representation of rapid assessment of HR and MMR status using tumor tissues immediately after surgery. **b** ADACHI Score and dMMR Score values determined using 21 tumor tissue samples from patients with brain tumors. Tumor samples preserved at 4 °C were dissociated into single-cell suspensions, and subjected to HR eye and MMR eye. **c** Western blot analysis for four MMR proteins using cells from patient BT#1 R. A172 cells (pMMR) and HT1080 cell lines (WT, *MLH1*$^{-/-}$, and *MSH2*$^{-/-}$) served as controls ($n = 1$). **d** ADACHI Score values determined by HR eye_1 or HR eye_2. Thirty-seven tumor tissue samples from patients with ovarian cancer (20 HGSC and 17 other types) were used. Samples preserved at 4 °C were dissociated into single-cell suspensions, and subjected to HR eye. HGSC, high-grade serous carcinoma. **e** Correlation between HR eye test results (ADACHI Score_1 or ADACHI Score_2) and myChoice® GI score. Note that GI score of ≥ 42 and/or the presence of a pathogenic *BRCA* mutation are defined as HRD in the myChoice® test[46]. OC#28 and OC#29 harbored a pathogenic *BRCA1* mutation (p.E1214* and p.K505Tfs*12, respectively), while OC#16 harbored a pathogenic *BRCA2* mutation (p.I605Yfs*9) (see Supplementary Fig. 16c). **f** Generation of HT1080 cell lines that ectopically express Rad51D or Rad51D_V66M. *RAD51D*$^{-/-}$ cells were generated by CRISPR/Cas9-mediated gene knockout, and a CMV promoter-driven expression vector for Rad51D or Rad51D_V66M was stably transfected into *RAD51D*$^{-/-}$ cells. Expression of Rad51D or Rad51D_V66M was confirmed by western blot analysis. Western blots shown are representative results from four independent experiments. **g** Analysis of HR status in Rad51D_V66M-expressing cells. Data shown are the mean ± s.d. of three independent experiments. **h** Sensitivity to PARPi and PolQi of Rad51D_V66M-expressing cells. Symbols are as in **g**. Data shown are the mean ± s.d. of three independent experiments. Where absent, error bars fall within symbols. Statistical significance in **g** and **h** was determined by one-way ANOVA with Dunnett's multiple comparisons. *$P < 0.05$; **$P < 0.01$; ns, not significant. Source data are provided as a Source Data file.

Ectopic expression of *RAD51D* in this mutant restored HR capacity and alleviated hypersensitivity to those drugs, while expression of a mutated *RAD51D* gene harboring p.V66M mutation did not exhibit such complementation (Fig. 6g, h). These results indicate that *RAD51D* p.V66M does cause HRD and that sample OC#4 M is an HRD tumor harboring a pathogenic mutation of *RAD51D*. Taken together, the results presented here suggest that the HR eye method, especially HR eye_2, can properly assess the HR status to an extent comparable or superior to existing clinical tests. It should also be emphasized again that, in addition to its validity and reliability, our method enables ultra-rapid (just 1-day) functional assessment of HR and MMR using frozen as well as refrigerated tissues without the need for non-tumor controls.

Discussion

Current diagnostic approaches to targeted therapies for HRD and dMMR tumors rely on "indirect" analysis and do not investigate actual DNA repair capacity, thus potentially compromising safe and proper application of effective targeted therapies[7,53] (Supplementary Figs. 1 and 2). Several approaches have been reported to functionally measure HR capacity without constructing a stable clone harboring recombination substrates, for example, using a Rad51 foci formation assay[54,55], a replication fork/DNA fiber assay[56], or qPCR analysis of gene-targeting frequency[57]. However, these methods, while potentially applicable to functional assay in tumor tissues, have several concerns and are technically challenging for clinical implementation. For example, although Rad51 foci formation assay is considered the most promising as a pre-clinical standard, this method still has some technical difficulties, requires drug-untreated controls, and lacks accuracy due to unclear thresholds (i.e., the distribution of RAD51-foci scoring is continuous, not bimodal)[13,14,58]. Similarly, although dMMR diagnosis is feasible with MSI or IHC analysis, these methods are still not fully reliable and do not represent the "gold standard": MSI tests are capable of causing false negative results[23], while IHC cannot detect amino acid substitutions of MMR proteins[59]. To the best of our knowledge, functional assays for detecting dMMR tumors without control cells/tissues have yet to be developed.

In this study, we have constructed various types of Nluc-based DNA constructs that, upon transfection, allow for extrachromosomal recombination, which led us to successfully develop cell-based "direct" functional assay systems to evaluate the status of HR, SSA, and MMR in cells and tissues (Figs. 1–4). Further, we have demonstrated the validity and utility of our systems, HR eye and MMR eye, as tools to evaluate the functional status of HR and MMR in tumor tissues derived from different types of solid tumors (Figs. 5 and 6). Extrachromosomal recombination between homologous DNA sequences was well studied when its molecular mechanisms and genetic requirements were unknown and the difference between HR and SSA was not argued or discussed[60,61]. The presented results show that ecHR and ecSSA are mechanistically and genetically distinct from one another, with the latter suppressed by MMR proteins, depending on the extent of sequence divergence between homeologous DNA substrates. We have also shown that extrachromosomal recombination events are mechanistically similar to chromosomal events. This may not be surprising, however, given that extrachromosomal DNA adopts a degree of chromatin structure[62]. In support of this notion, when this paper was in preparation, a similar observation was reported that ecHR and ecSSA can be monitored using transient transfection of recombination substrates[63]. It should be noted, however, that the study only used a limited number of cell lines and did not employ tumor tissues. Additionally, absolute scoring of DNA repair status was not attempted or discussed, and the impact of MMR on ecSSA was not investigated. Our methods, HR eye and MMR eye, are based on the use of Nluc as a reporter gene and a high-efficiency transfection system, which were the key to successful absolute scoring of HR and MMR.

Notably, we have shown in this study that not only does HR eye enable rapid assessment of HR capacity within a day (~25 h after tissue dissociation) but also can predict the efficacy of PARPi and PolQi with no need for testing control cells (Fig. 3d). Moreover, to our surprise, HR eye-based ADACHI Score values can properly assess the actual state of HR in cells that do not harbor apparent HR gene mutations as well as in cells that have acquired PARPi resistance. Indeed, Myc/Mycn-overexpressing cells were properly judged as HRD (Fig. 3b), as could not have been performed by existing NGS-based diagnostic strategies (Supplementary Fig. 1). More intriguingly, we have demonstrated that a *RAD51D* VUS mutation, p.V66M, is indeed an HRD-causing pathogenic mutation (Fig. 6g, h). This finding was triggered by a reliable result of HR eye that revealed a high ADACHI Score value in one patient biopsy harboring this mutation (OC#4 M), which was clinically diagnosed as HRP in FoundationOne® as well as in myChoice®. This implies that the HR eye method is comparable or superior to existing clinical tests. Hence, the HR eye method has the potential to offer a tool to improving precision medicine associated with synthetic lethality-based HRD cancer therapy. It would be particularly advantageous to provide a rapid determination for tumors under PARPi treatment and for rapidly progressing tumors such as pancreatic cancer.

We have also demonstrated that the MMR eye method allows rapid assessment of MMR status in actual tumor tissues (Fig. 6a, b). It is important to note that MMR loss does not necessarily lead to MSI-High or TMB-High[23,24]. The dMMR status is frequently caused by promoter methylation of an MMR gene(s)[64]. Such dMMR tumors due to epigenetic silencing cannot be assessed by current analysis relying on NGS (Supplementary Fig. 2), highlighting the merit of MMR eye because it rapidly determines the correct status of MMR in tumors, including those recurrently arise during TMZ treatment[43,65].

Notably, our methods permit the use of frozen tumor tissues after long-term (up to 1 week) storage. Thus, the requirement of live tissue biopsies is not a limitation toward clinical implementation. However, one important issue remains to be addressed. Although the ultra-rapid (1-day) assessment of HRD/dMMR tumors without the need for non-tumor controls is a step forward, we noticed that tumor tissues from mouse models had a tendency to generate a slightly lower Score value than in vitro-cultured original cells (Fig. 5b). Further, the perfect bimodal distribution of Score values of repair-deficient and proficient cell populations (note that such bimodal distribution has never been observed in the myChoice® test or Rad51 foci formation assay) were somewhat less evident in actual ovarian cancer tissues, although HR eye_2 still allowed accurate determination of the correct status for HRD tumors (Fig. 6e). We speculate that this slight discrepancy between in vitro and in vivo results is attributed to intratumor heterogeneity or low tumor cellularity. Intratumor heterogeneity is a well-recognized characteristic of tumors[66], and genetic or epigenetic diversity can be seen in various parts of the same tumor[67,68]. When using formalin-fixed paraffin-embedded (FFPE) samples, it is technically possible to choose a "convenient" site for genetic analysis, yet even in myChoice®, the same tumor could be judged as HRP or HRD depending on the biopsy site sampled[69,70]. In contrast, our method is based on dissociating the whole tumor tissue being tested and therefore contamination of "inconvenient" parts would be unavoidable. In terms of intratumor heterogeneity, however, such "impartial" testing using the whole tumor tissue may rather be beneficial to understand the true status of DNA repair and to predict the effectiveness of chemotherapy, targeted therapy and immunotherapy. A major problem of tumor heterogeneity applies to efficient targeted therapy as well as accurate diagnosis[44,53,71]. In this respect, our finding that ADACHI Score values display a high correlation to sensitivity to PARPi (as well as PolQi and cisplatin) is quite intriguing, because even tumors with a Score value of <1 would contain a substantial number of drug-sensitive cancer cells. This is particularly true for olaparib, the cellular sensitivity to

which exhibits a strong linear correlation with HR eye-based ADACHI Score (see Fig. 3d). Thus, beyond its accuracy for HRD prediction, the HR eye method may be relevant as a therapeutic biomarker for predicting drug efficacy and safety.

In general, FDA-approved clinical tests using the FFPE sample typically need ≥ 20% tumor content to obtain reliable results (e.g., myChoice®, FoundationOne®, or MI Cancer Seek™)[46,72,73]. Our experiments using intentionally mixed cell lines implied that HR eye would recommend ≥ 50% tumor content for HRD determination, while MMR eye ≥ 30% tumor content for dMMR determination (Fig. 5d, e and Supplementary Fig. 14a, c). These estimates could be harsh assessments for testing patient biopsies, assuming the aforementioned possibility that <1 ADACHI/dMMR Score values still represent HRD/dMMR status for tumor tissues with low tumor content. Indeed, HR eye_2 allowed accurate determination of HRD status for essentially all tumors that were diagnosed as HRD or misjudged as HRP in myChoice® test (Fig. 6e). Intriguingly, in our analysis using ovarian cancer tissues, two samples that had undergone standard chemotherapy displayed very low transfection efficiency, which we speculate is due to the low number of viable cells. Given this, it is tempting to argue that, unlike FFPE-based clinical tests, the HR eye/MMR eye methods do not need advance confirmation of tumor content, with the exception of chemotherapy-treated tumors judged as HRP/pMMR. Those tumors with an insufficient number of viable cancer cells could be tested in parallel using FFPE samples (for example, myChoice®, if available, for HRD testing). Alternatively, this issue could be overcome by employing a tissue-specific or cancer-specific gene promoter for conditional Nluc expression, thereby improving accuracy of HR eye/MMR eye testing for those low-transfection-efficiency tissues. Because tumor cellularity as well as intratumor heterogeneity would vary among tumor tissues as well as among solid tumors[44,45,74], a more comprehensive study, preferably for each type of cancer, needs to be conducted to address all the issues discussed above.

We emphasize that the clinical significance of scoring DNA repair abnormalities and reliably predicting the efficacy of molecular targeted therapy is substantial, making a contribution to the advancement of precision medicine[75]. Therefore, it is anticipated that the HR eye and MMR eye strategies could be clinically applied to ovarian cancer and eventually other solid tumors. The development of highly accurate companion diagnostics will increase the number of patients who can benefit from efficient targeted therapies aimed at HRD and dMMR tumors. In this regard, it should be mentioned that these tumors are highly frequent and tissue-agnostic[1,2,15,16]; additionally, a recent report suggested a significant decrease in HR and MMR activity in BRAFi/EGFRi-treated colorectal cancers[76], further highlighting the importance of rapid assessment of DNA repair status of tumors including those that were originally DNA repair-proficient. Finally, cell-based functional assays using live cells from resected tissues may be an effective approach not only for assessing DNA repair status but also for other diagnostic purposes and possibly as a first-level prediction of drug efficacy.

Methods

Ethical statement

All animal experiments were approved by the Institutional Animal Care and Use Committee (Unitech Co., Ltd., Chiba, Japan, AGR YID-210407A-20, AGR YID-211007A-20, AGR YID-211217A-27, and AGR YID-221214A-28; Yokohama City University, Yokohama, Japan, F-A-21-053 and F-A-22-011). The condition of mice was continuously monitored, and the mice were sacrificed when the tumor weight was determined to exceed 10% of the body weight, when tumor size reached 20 mm, when more than 20% weight loss was observed, or when the general or neurological condition met the criteria for euthanasia.

All experiments using patient biopsies were performed in accordance with the Declaration of Helsinki and approved by the Institutional Review Board [Yokohama City University (YCU) IRB numbers: A171130006 and F230600007]. Written informed consent was obtained from all the patients. The patient's sex/gender was determined based on self-reporting and not considered in the selection of patients. Overall, 21 brain tumor samples from 20 patients (8 males and 12 females, aged from 21 to 81) and 37 ovarian tumor samples from 34 patients (34 females, aged from 41 to 79) were used in this study.

Cell culture

The cell lines used are summarized in Supplementary Table 1. All cells were cultured in a humidified atmosphere of 5% CO_2 incubator at 37 °C, and tested for mycoplasma contamination using a Venor®GeM OneStep Mycoplasma Detection Kit (Minerva Biolabs Inc., Berlin, Germany). HT1080, HeLa S3, HCT116, and U2OS cells were cultured in Dulbecco's Modified Eagle Medium (Shimadzu Diagnostics Co., Tokyo, Japan) supplemented with 10% (for HeLa, 5%) heat-inactivated calf serum (Cytiva, Tokyo, Japan) or fetal bovine serum (Biowest, Nuaillé, France). HEC59, HCC1937, Capan-1, OVSAHO, and Nalm-6 cells were cultured in Eagle's Minimum Essential Medium (MEM; Shimadzu Diagnostics Co., Tokyo, Japan) supplemented with 10% heat-inactivated calf serum, MEM Non-Essential Amino Acids Solution (FUJIFILM Wako Pure Chemical, Osaka, Japan), 1 mM sodium pyruvate, 50 μM 2-mercaptoethanol (FUJIFILM Wako Pure Chemical), and 0.15 μM vitamin B12 (Sigma-Aldrich)[34]. DLD1, MDA-MB-468, and MDA-MB-436 cells were cultured in RPMI-1640 medium (FUJIFILM Wako Pure Chemical) supplemented with 10% heat-inactivated calf serum. UWB1.289 cells were cultured in 50% Mammary Epithelial Growth Medium (MEGM Bullet Kit; Lonza, Basel, Switzerland) and 50% RPMI-1640 medium supplemented with heat-inactivated 3% fetal bovine serum. Patient-derived glioma tumorsphere lines (MGG4, MGG18, MGG123, MGG152 and TMZ-resistant MGG152 cells) were cultured in Neurobasal Medium (Thermo Fisher Scientific, Waltham, MA, USA) supplemented with 1 x GlutaMax (Thermo Fisher Scientific), 1 x B27 Supplement (Thermo Fisher Scientific), 1 x N2 Supplement (Thermo Fisher Scientific), 20 ng/ml EGF (R&D Systems, Minneapolis, MN, USA or FUJIFILM Wako Pure Chemical), 20 ng/ml bFGF (Alomone Labs, Jerusalem, Israel or FUJIFILM Wako Pure Chemical), and 1 x Penicillin-Streptomycin Solution (Thermo Fisher Scientific)[43,77–79].

Transfection

Transfection using the MaxCyte STX device (MaxCyte, Rockville, MD, USA) was performed according to the manufacturer's instructions. Briefly, 0.5–2 ×10^6 cells were suspended in 25 μl of the supplied solution (MaxCyte Electroporation Buffer) and transfected with 0.25–1 μg of DNA[34]. Transfection using the GTE-1 electroporation apparatus (Shimadzu, Kyoto, Japan) was performed according to the manufacturer's instructions. Briefly, cells were washed twice with Saline G (130 mM NaCl, 5.3 mM KCl, 1.1 mM Na_2HPO_4, 1.1 mM KH_2PO_4, 6.1 mM glucose, 0.49 mM $MgCl_2$ and 0.9 mM $CaCl_2$) and an aliquot of cell suspension (4 × 10^6 cells in 40 μl of Saline G) was electroporated with 4 μg of DNA[34]. Transfection using jetPEI transfection reagent (Polyplus-transfection, Illkirch, France) was performed according to the manufacturer's instructions. Briefly, 1 × 10^5 cells were plated onto 6-well dish, cultured for 24 h, and treated with DNA/jetPEI complexes.

HR-Nluc and SSA-Nluc constructs

Nluc-based recombination substrates were artificially synthesized (Thermo Fisher Scientific; GenScript Japan K.K., Tokyo, Japan) or PCR amplified with PrimeSTAR HS DNA Polymerase (Takara Bio, Otsu, Japan) using pNL1.1[Nluc] (Promega, Fitchburg, WI, USA) as a template. These fragments were subcloned into pCMV-Nluc[34] or pUC19 (Takara Bio) using In-Fusion®HD Cloning Kit (Clontech, Mountain View, CA, USA) and standard molecular biology techniques. Correct DNA assembly was confirmed by restriction mapping and sequencing

(Eurofins Genomics K.K., Tokyo, Japan). All Nluc-based DNA constructs are depicted in Supplementary Figs. 3a, 7c, and 8a–c, and the details of vector construction are available upon request.

Cell-based functional assay using HR-Nluc and SSA-Nluc constructs

An HR-Nluc or SSA-Nluc construct was transfected into cells using the MaxCyte STX device. After a 1, 2, 4, 8, 12, or 24-hour incubation, an aliquot (~5 $\times 10^5$ cells) was suspended in 50 µl of PBS and luciferase activity was measured using the Nano-Glo Luciferase Assay System (Promega) according to the manufacturer's instructions. pCMV-Nluc was used as a control plasmid. For HR-Nluc-v2, an equimolar mixture of pCMV-GapNluc and pUC-iNluc was used. Similarly, an equimolar mixture of pCMV-GapNluc and iNluc fragment, or an equimolar mixture of pCMV-GapNluc-v2, iNluc5′ fragment, and iNluc3′ fragment was used for SSA-Nluc-v2 and v3, respectively.

All the plasmid vectors were purified with Qiagen Plasmid *plus* Midi Kits (Qiagen K.K., Tokyo, Japan). The iNluc, iNluc5′, and iNluc3′ fragments were purified with Wizard® SV Gel and PCR Clean-Up System (Promega) prior to transfection. pCMV-Nluc and pUC-iNluc were used in a circular form, and the other constructs were linearized with an appropriate restriction enzyme prior to transfection.

HT1080 mutant cell lines

MSH2$^{-/-}$ HT1080 cells have been described previously[30]. *MLH1*$^{-/-}$ and *RAD51D*$^{-/-}$ cells were generated by CRISPR/Cas9-mediated gene knockout. An all-in-one CRISPR vector, pX330-U6-Chimeric_BB-CBh-hSpCas9 (Addgene plasmid #42230)[80], was used to express Cas9 and single-guide RNA. Sense and antisense oligonucleotides of each single-guide RNA targeting sequence were annealed and cloned into pX330-U6-Chimeric_BB-CBh-hSpCas9 at the BbsI site. The CRISPR-Cas9 target sequence for *MLH1* knockout was 5′-AGTGGTGAACCG-CATCGCGGCGG-3′, and for *RAD51D* knockout was 5′-AGA-GATCAGCGCCATTCACGGGG-3′ (20 bp target and 3 bp PAM sequence (underlined)). *MLH1* or *RAD51D* gene disruption was screened using primers MLH1-Del-Check-Fw and MLH1-Del-Check-Rv, or Rad51D-Del-Check-Fw and Rad51D-Del-Check-Rv, respectively (Supplementary Table 2). The PCR products were cloned into pTAKN2 T-Vector (Bio-Dynamics Laboratory Inc., Tokyo, Japan) to determine the sequence (Eurofins Genomics K.K.). The absence of *MLH1* or *RAD51D* expression was verified by western blot analysis. To generate a cell line with ectopic expression of Rad51D or Rad51D_V66M, an CMV promoter-driven *RAD51D* or *RAD51D_V66M* expression vector (see below) was linearized with AhdI and transfected into *RAD51D*$^{-/-}$ cells. After a 2-week cultivation, G418-resistant colonies were isolated and subjected to western blot analysis.

Nalm-6 mutant cell lines

The *MSH2*-corrected Nalm-6 cell line has been described previously[81]. All gene-knockout mutant cell lines were generated by conventional gene targeting without using CRISPR/Cas9. Targeting vectors for disruption of the *FANCA, TP53BP1*, and *MLH1* genes (listed in Supplementary Table 3) were constructed by standard molecular biology techniques, and the details of vector construction are available upon request. Primers used to confirm correct gene-targeting events are listed in Supplementary Table 2. *RAD54*$^{-/-}$, *RAD54*$^{-/-}$*RAD54B*$^{-/-}$, *RAD52*$^{-/-}$, *LIG4*$^{-/-}$, *POLQ*$^{-/-}$, *LIG4*$^{-/-}$*POLQ*$^{-/-}$, and *LEDGF*$^{-/-}$ cells have been described previously[34,82–85]. The knockout status of these cells was verified by PCR and western blot analysis.

Creation of *MSH2*-corrected HEC59 cells

Restoration of MSH2 expression in HEC59 cells was performed essentially as described[81]. Briefly, PmeI-linearized pMSH2-Neo was MaxCyte transfected into HEC59 cells, and G418-resistant colonies were expanded to prepare genomic DNA. Correct gene-targeting events were PCR screened using primers MSH2 GT-Fw and 3′-loxP (Supplementary Table 2). The restoration of Msh2/Msh6 expression was confirmed by western blot analysis.

Isolation of olaparib-resistant clones from MDA-MB-436

Olaparib-resistant MDA-MB-436 clones were established essentially as described[86]. Briefly, MDA-MB-436 cells were cultured for 3 weeks in growth medium containing 10 nM olaparib, and the resulting colonies were isolated and assayed for HR status. HR-restored cell lines were subjected to drug sensitivity and cell survival assays.

Cell survival assay

MDA-MB-436 and Nalm-6 cells were transfected twice in an interval of 48 h with a *DT-A*-linked HR-Nluc-DTA construct using the MaxCyte STX device or jetPEI transfection reagent. After a 72-hour incubation, cell growth was measured using the CellTiter-Glo Luminescent Cell Viability Assay Kit (Promega) as previously described[82]. For HR-Nluc-DTA-v2, an equimolar mixture of pCMV-GapNluc-2A-DTA and pUC-iNluc was transfected. pCMV-Nluc and pCMV-Nluc-2A-DTA were used as controls in each assay. pCMV-Nluc, pCMV-Nluc-2A-DTA, and pUC-iNluc were used as a circular plasmid, and the other constructs were linearized with an appropriate restriction enzyme prior to transfection.

Xenograft models

HCT116 and HEC59 xenograft models: Cells (2–6 $\times 10^6$) were subcutaneously implanted to 6- to 8-week-old female BALB/cAJcl nude mice (CLEA Japan, Inc., Tokyo, Japan). After 3 weeks, tumor tissues were isolated and dissociated into single-cell suspensions using a combination of the gentleMACS Dissociator (Miltenyi Biotec, Bergisch Gladbach, Germany) and the Tumor Dissociation Kit, human (Miltenyi Biotec), according to the manufacturer's instructions.

MDA-MB-436 xenograft models: Cells (2–6 × 10^6) were orthotopically implanted into the right mammary gland of 6- to 8-week-old female BALB/cAJcl nude mice (CLEA Japan, Inc.). After 4 weeks, tumor tissues were isolated and dissociated as above.

Glioma xenograft models: Dissociated tumor cells (1–2 $\times 10^5$) derived from patient tumor specimens (YMG56, YMG62, YMG67, YMG117R, YMG151R, and YMG227) or established glioma tumorsphere lines (MGG4, MGG18, MGG123, and MGG152; kindly provided by Massachusetts General Hospital) were implanted into the right striatum of 4 to 7-week-old female SCID Beige mice (Charles River, Yokohama, Japan). The brains were harvested for pathologic studies and for acutely dissociated tumor cells that were cryopreserved and subjected to in vitro experiments.

Orthotopic pancreatic cancer mouse model: Pancreatic cancer organoids harboring *Kras* and *Trp53* mutations (*Kras*^{G12D} and *Trp53*$^{-/-}$) were orthotopically implanted into the pancreas of 6-week-old C57BL/6 J wild-type mice (CLEA Japan, Inc., Tokyo, Japan) essentially as described[87,88]. Pancreatic tumors were harvested after 4 weeks and subjected to in vitro experiments.

Collection and processing of patient-derived tumor tissues

The patients with brain tumors (Supplementary Fig. 15b) or ovarian cancer (Supplementary Fig. 16c) who underwent surgery at the YCU Hospital were enrolled in this study. Surgically resected brain tumor tissues were stored in the MACS Tissue Storage Solution (Miltenyi Biotec) at 4 °C in a cryovial. Likewise, surgically resected ovarian cancer tissues were further divided into 3-5 mm pieces. Unfrozen, refrigerated specimens were stored in the MACS Tissue Storage Solution (Miltenyi Biotec) at 4 °C. Frozen specimens were stored in Bambanker® freezing medium (NIPPON Genetics, Tokyo, Japan) at −80 °C.

After storage, tumor specimens were dissociated into single-cell suspensions. The cells were suspended in culture medium (for brain tumors, the same medium as for the patient-derived glioma

tumorsphere lines; for ovarian cancer, RPMI-1640 medium supplemented with 10% heat-inactivated fetal bovine serum) and subjected to HR eye and MMR eye, as illustrated in Fig. 6a.

Genomic analysis of tumor samples

Genomic DNA was extracted from surgical specimens (YMG56, YMG67, and BT#1 R) using the DNeasy Blood & Tissue Kit (Qiagen K.K.) according to the manufacturer's protocol. For YMG56 and YMG67, four MMR genes (*MSH2*, *MSH6*, *MLH1*, and *PMS2*) were analyzed for genetic mutations (single nucleotide variants, small insertions/deletions, and copy number variants) by the Multiplex PCR-based MGH SNaPshot assay as described previously[89]. For BT#1 R, BT#3, BT#12, and BT#20 R (FoundationOne®; Chugai Pharmaceutical, Tokyo, Japan) was used for genomic profiling.

For ovarian tumor samples, FFPE samples were subjected to myChoice® (Myriad Genetic Laboratories, Inc.) or FoundationOne® (Chugai Pharmaceutical).

siRNAs and shRNA expression vectors

All chemically synthesized siRNAs were purchased from Horizon Discovery (MSH2 siRNA, L-003909-00; MLH1 siRNA, L-003906-00; MSH6 siRNA, L-019287-00; PMS2 siRNA, L-010032-00). DNA fragments containing shRNA-coding sequence (5′-CGGTCAGAGATCATACAGATT-3′ for *RAD51*, and 5′-CCTAAGGTTAAGTCGCCCT-3′ for control) were prepared by annealing two oligonucleotides shRad51-top and shRad51-btm, or shCtrl-top and shCtrl-btm, respectively (Supplementary Table 2). Each DNA fragment was cloned into pBAsi-hU6 Neo (Takara Bio) to generate an shRNA expression vector.

Rad51D expression vectors

An expression vector for the human *RAD51D* gene was constructed using In-Fusion®HD Cloning Kit. Briefly, a 1036-bp DNA fragment containing Rad51D cDNA was PCR amplified with PrimeSTAR HS DNA Polymerase using pFN21A HaloTag® CMV Flexi® Vector_human RAD51D (FHC06580; Promega) as a template. The primers used were Rad51D-Fw and Rad51D-Rv (Supplementary Table 2). The PCR fragment and an NheI/XbaI-digested pIRES vector (Takara Bio) were subjected to In-Fusion cloning, yielding pCMV-Rad51D. Using this plasmid, construction of pCMV-Rad51D-V66M was performed using a PCR-based site-directed mutagenesis with four primers shown in Supplementary Table 2.

GFP reporter assay

The DR-GFP/SA-GFP reporter cassettes[35,36] were inserted at exon 3 of the *HPRT* gene by gene targeting, and GFP reporter assays were performed as previously described[90,91]. Briefly, cells were transfected with I-SceI expression vector pSceI or the GFP expression vector pmaxGFP (Lonza) using the MaxCyte STX device. Cells were then cultured for 72 h, and GFP-positive cells were counted using an Attune Nxt Flow Cytometer (Thermo Fisher Scientific, Waltham, MA, USA). For the transient assay, cells were MaxCyte transfected with I-SceI-linearized pHPRT-DR-GFP or pHPRT-SA-GFP. After a 1, 2, 4, 8, 12, 24, 48, or 72-hour incubation, GFP-positive cells were counted as above. In each experiment, 1–5 $\times 10^5$ cells were analyzed, and the percentage of GFP-positive cells was calculated from the number of GFP-positive cells divided by the number of cells analyzed.

Chemicals

Puromycin, hygromycin B, G418, cisplatin, and novobiocin were purchased from FUJIFILM Wako Pure Chemical and dissolved in distilled water. Talazoparib (BMN673), ART558, and RP-6685 were purchased from MedChemExpress (Monmouth Junction, NJ, USA) and dissolved in dimethyl sulfoxide. Olaparib, niraparib, etoposide, and temozolomide (TMZ) were purchased from Selleck Chemicals (Houston, TX, USA) and dissolved in dimethyl sulfoxide. O^6-benzylguanine (O^6-BG) and camptothecin were purchased from Sigma-Aldrich (St. Louis, MO, USA) and dissolved in dimethyl sulfoxide.

Clonogenic survival assay

Cellular sensitivity to anticancer drugs was determined by clonogenic survival assay as essentially described[30,86,92–95]. Briefly, 10^4–10^6 cells were seeded into 6-well plate, and various concentrations of anticancer drugs were added to the medium after 24 h. Cells were allowed to grow for 1 to 2 weeks, and colonies were stained with 0.1% crystal violet (FUJIFILM Wako Pure Chemical) for 30 min. The stained colonies were quantified using ImageJ Software. For experiments using TMZ, 5 μM O^6-benzylguanine, an inhibitor of O^6-methylguanine-DNA methyltransferase (MGMT), was added to the medium to enhance the cytotoxic effect of TMZ.

Western blot analysis

Cells (2–10 $\times 10^6$) were washed twice with PBS^- and scraped in 150 μl of lysis buffer (50 mM Tris-HCl (pH 6.8), 2% sodium dodecyl sulfate, 10% glycerol, 100 μM dithiothreitol, 1 mM phenylmethylsulfonyl fluoride) containing Protease Inhibitor Cocktail (Sigma-Aldrich). The lysates were allowed to stand for 20 min at 4 °C and, after sonication, centrifuged at 21,500 x *g* for 30 min at 4 °C. The supernatants were collected and used for western blot analysis. Protein concentration was determined using the Protein Assay BCA Kit (FUJIFILM Wako Pure Chemical). Fifteen micrograms of the lysates were electrophoresed in a 7.5% polyacrylamide gel or a 5–15% gradient polyacrylamide gel (Funakoshi, Tokyo, Japan) and then transferred onto a polyvinylidene difluoride membrane (Merck Millipore). Membranes were blocked with 5% skim milk and then incubated with a primary antibody, followed by incubation with a horseradish peroxidase-conjugated secondary antibody. Signals were detected with Clarity Western ECL Substrate (Bio-Rad, Hercules, CA, USA) and analyzed using a Fuji Image Analyzer LAS-1000UVmini (FUJIFILM Co., Tokyo, Japan). The antibodies used are listed in Supplementary Table 4. Full scans of the blots are shown in Source Data file.

Statistics & reproducibility

Data analysis was performed using GraphPad Prism (version 8.4.3) and Microsoft Excel (version 16.16.11). A *P* value less than 0.05 was considered significant. All experiments were independently replicated, as described in each figure legend, and no data was excluded from the study.

Reporting summary

Further information on research design is available in the Nature Portfolio Reporting Summary linked to this article.

Data availability

All data that support the findings of this study are available within the article. Source data are provided with this paper.

References

1. Heeke, A. L. et al. Prevalence of homologous recombination-related gene mutations across multiple cancer types. *JCO Precis. Oncol.* **2**, 2018 (2018).
2. Nguyen, L., Martens, J. W. M., Van Hoeck, A. & Cuppen, E. Pan-cancer landscape of homologous recombination deficiency. *Nat. Commun.* **11**, 5584 (2020).
3. Lord, C. J. & Ashworth, A. BRCAness revisited. *Nat. Rev. Cancer* **16**, 110–120 (2016).
4. Helleday, T. Homologous recombination in cancer development, treatment and development of drug resistance. *Carcinogenesis* **31**, 955–960 (2010).
5. Lord, C. J. & Ashworth, A. PARP inhibitors: Synthetic lethality in the clinic. *Science* **355**, 1152–1158 (2017).

6. Higgins, G. S. & Boulton, S. J. Beyond PARP-POLθ as an anticancer target. *Science* **359**, 1217–1218 (2018).
7. Makin, S. What's next for PARP inhibitors? *Nature* **600**, 36–38 (2021).
8. Konstantinopoulos, P. A., Ceccaldi, R., Shapiro, G. I. & D'Andrea, A. D. Homologous recombination deficiency: Exploiting the fundamental vulnerability of ovarian cancer. *Cancer Discov* **5**, 1137–1154 (2015).
9. Telli, M. L. et al. Homologous recombination deficiency (HRD) score predicts response to platinum-containing neoadjuvant chemotherapy in patients with triple-negative breast cancer. *Clin. Cancer Res.* **22**, 3764–3773 (2016).
10. Marquard, A. M. et al. Pan-cancer analysis of genomic scar signatures associated with homologous recombination deficiency suggests novel indications for existing cancer drugs. *Biomark. Res.* **3**, 9 (2015).
11. Lengauer, C., Kinzler, K. W. & Vogelstein, B. Genetic instabilities in human cancers. *Nature* **396**, 643–649 (1998).
12. Noordermeer, S. M. & van Attikum, H. PARP inhibitor resistance: A tug-of-war in BRCA-mutated cells. *Trends Cell Biol* **29**, 820–834 (2019).
13. van Wijk, L. M., Nilas, A. B., Vrieling, H. & Vreeswijk, M. P. G. RAD51 as a functional biomarker for homologous recombination deficiency in cancer: a promising addition to the HRD toolbox? *Exp. Rev. Mol. Diagn.* **22**, 185–199 (2022).
14. Miller, R. E. et al. ESMO recommendations on predictive biomarker testing for homologous recombination deficiency and PARP inhibitor benefit in ovarian cancer. *Ann. Oncol.* **31**, 1606–1622 (2020).
15. Le, D. T. et al. Mismatch repair deficiency predicts response of solid tumors to PD-1 blockade. *Science* **357**, 409–413 (2017).
16. Lorenzi, M., Amonkar, M., Zhang, J., Mehta, S. & Liaw, K.-L. Epidemiology of microsatellite instability high (MSI-H) and deficient mismatch repair (dMMR) in solid tumors. *J. Oncol.* **2020**, 1807929 (2020).
17. Jiricny, J. The multifaceted mismatch-repair system. *Nat. Rev. Mol. Cell Biol.* **7**, 335–346 (2006).
18. Hause, R. J., Pritchard, C. C., Shendure, J. & Salipante, S. J. Classification and characterization of microsatellite instability across 18 cancer types. *Nat. Med.* **22**, 1342–1350 (2016).
19. Chalmers, Z. R. et al. Analysis of 100,000 human cancer genomes reveals the landscape of tumor mutational burden. *Genome Med* **9**, 34 (2017).
20. Yarchoan, M., Hopkins, A. & Jaffee, E. M. Tumor mutational burden and response rate to PD-1 Inhibition. *N. Engl. J. Med.* **377**, 2500–2501 (2017).
21. Samstein, R. M. et al. Tumor mutational load predicts survival after immunotherapy across multiple cancer types. *Nat. Genet.* **51**, 202–206 (2019).
22. Stupp, R. et al. Radiotherapy plus concomitant and adjuvant temozolomide for glioblastoma. *N. Engl. J. Med.* **352**, 987–996 (2005).
23. Wang, Y., Shi, C., Eisenberg, R. & Vnencak-Jones, C. L. Differences in microsatellite instability profiles between endometrioid and colorectal cancers: A potential cause for false-negative results? *J. Mol. Diagn.* **19**, 57–64 (2017).
24. Quintanilha, J. C. F. et al. Comparative effectiveness of immune checkpoint inhibitors vs chemotherapy in patients with metastatic colorectal cancer with measures of microsatellite instability, mismatch repair, or tumor mutational burden. *JAMA Netw. Open* **6**, e2252244 (2023).
25. Kuchenbaecker, K. B. et al. Risks of breast, ovarian, and contralateral breast cancer for BRCA1 and BRCA2 mutation carriers. *JAMA* **317**, 2402–2416 (2017).
26. Lynch, H. T., Snyder, C. L., Shaw, T. G., Heinen, C. D. & Hitchins, M. P. Milestones of Lynch syndrome: 1895-2015. *Nat. Rev. Cancer* **15**, 181–194 (2015).
27. Luchini, C. et al. ESMO recommendations on microsatellite instability testing for immunotherapy in cancer, and its relationship with PD-1/PD-L1 expression and tumour mutational burden: a systematic review-based approach. *Ann. Oncol.* **30**, 1232–1243 (2019).
28. Bhargava, R., Onyango, D. O. & Stark, J. M. Regulation of single-strand annealing and its role in genome maintenance. *Trends Genet* **32**, 566–575 (2016).
29. Mladenov, E., Paul-Konietzko, K., Mladenova, V., Stuschke, M. & Iliakis, G. Increased gene targeting in hyper-recombinogenic lymphoblastoid cell lines leaves unchanged dsb processing by homologous recombination. *Int. J. Mol. Sci.* **23**, 9180 (2022).
30. Saito, S. & Adachi, N. Characterization and regulation of cell cycle-independent noncanonical gene targeting. *Nat. Commun.* **15**, 5044 (2024).
31. Baumann, P. & West, S. C. Role of the human RAD51 protein in homologous recombination and double-stranded-break repair. *Trends Biochem. Sci.* **23**, 247–251 (1998).
32. Symington, L. S. Role of RAD52 epistasis group genes in homologous recombination and double-strand break repair. *Microbiol. Mol. Biol. Rev.* **66**, 630–670 (2002).
33. Prakash, R., Zhang, Y., Feng, W. & Jasin, M. Homologous recombination and human health: the roles of BRCA1, BRCA2, and associated proteins. *Cold Spring Harb. Perspect. Biol.* **7**, a016600 (2015).
34. Saito, S., Maeda, R. & Adachi, N. Dual loss of human POLQ and LIG4 abolishes random integration. *Nat. Commun.* **8**, 16112 (2017).
35. Pierce, A. J., Johnson, R. D., Thompson, L. H. & Jasin, M. XRCC3 promotes homology-directed repair of DNA damage in mammalian cells. *Genes Dev* **13**, 2633–2638 (1999).
36. Stark, J. M., Pierce, A. J., Oh, J., Pastink, A. & Jasin, M. Genetic steps of mammalian homologous repair with distinct mutagenic consequences. *Mol. Cell. Biol.* **24**, 9305–9316 (2004).
37. Elstrodt, F. et al. BRCA1 mutation analysis of 41 human breast cancer cell lines reveals three new deleterious mutants. *Cancer Res* **66**, 41–45 (2006).
38. Ning, J. F. et al. Myc targeted CDK18 promotes ATR and homologous recombination to mediate PARP inhibitor resistance in glioblastoma. *Nat. Commun.* **10**, 2910 (2019).
39. Sugawara, N., Goldfarb, T., Studamire, B., Alani, E. & Haber, J. E. Heteroduplex rejection during single-strand annealing requires Sgs1 helicase and mismatch repair proteins Msh2 and Msh6 but not Pms1. *Proc. Natl. Acad. Sci. USA* **101**, 9315–9320 (2004).
40. Spies, M. & Fishel, R. Mismatch repair during homologous and homeologous recombination. *Cold Spring Harb. Perspect. Biol.* **7**, a022657 (2015).
41. Trost, H., Merkell, A., Lopezcolorado, F. W. & Stark, J. M. Resolution of sequence divergence for repeat-mediated deletions shows a polarity that is mediated by MLH1. *Nucleic Acids Res* **51**, 650–667 (2023).
42. Huang, R. & Zhou, P. K. DNA damage repair: historical perspectives, mechanistic pathways and clinical translation for targeted cancer therapy. *Signal Transduct. Target. Ther.* **6**, 254 (2021).
43. Tateishi, K. et al. The alkylating chemotherapeutic temozolomide induces metabolic stress in IDH1-mutant cancers and potentiates NAD(+) depletion-mediated cytotoxicity. *Cancer Res* **77**, 4102–4115 (2017).
44. Garattini, S., Fuso Nerini, I. & D'Incalci, M. Not only tumor but also therapy heterogeneity. *Ann. Oncol.* **29**, 13–19 (2018).
45. Hatakeyama, K. et al. Tumor mutational burden analysis of 2,000 Japanese cancer genomes using whole exome and targeted gene panel sequencing. *Biomed. Res.* **39**, 159–167 (2018).
46. myCHOICE CDx technical information. FDA. https://www.accessdata.fda.gov/cdrh_docs/pdf19/P190014S003C.pdf (2020).
47. ClinVar: public archive of relationships among sequence variation and human phenotype. NCBI. https://www.ncbi.nlm.nih.gov/clinvar/RCV000130161/ (2021).

48. LOVD v.2.0: the next generation in gene variant databases. Leiden University Medical Center. https://databases.lovd.nl/shared/variants/0000561045#00017371 (2023).
49. Greenhough, L. A. et al. Structure and function of the RAD51B-RAD51C-RAD51D-XRCC2 tumour suppressor. *Nature* **619**, 650–657 (2023).
50. Takata, M. et al. Chromosome instability and defective recombinational repair in knockout mutants of the five Rad51 paralogs. *Mol. Cell. Biol.* **21**, 2858–2866 (2001).
51. Hatanaka, A. et al. Similar effects of Brca2 truncation and Rad51 paralog deficiency on immunoglobulin V gene diversification in DT40 cells support an early role for Rad51 paralogs in homologous recombination. *Mol. Cell. Biol.* **25**, 1124–1134 (2005).
52. Bhattacharya, D. et al. RAD51 paralogs: Expanding roles in replication stress responses and repair. *Curr. Opin. Pharmacol.* **67**, 102313 (2022).
53. de Lartigue, J. HRD testing heralds a new biomarker, but questions linger. *Oncol. Live* **21**, 15 (2020).
54. Naipal, K. A. et al. Functional ex vivo assay to select homologous recombination-deficient breast tumors for PARP inhibitor treatment. *Clin. Cancer Res.* **20**, 4816–4826 (2014).
55. Cruz, C. et al. RAD51 foci as a functional biomarker of homologous recombination repair and PARP inhibitor resistance in germline BRCA-mutated breast cancer. *Ann. Oncol.* **29**, 1203–1210 (2018).
56. Hill, S. J. et al. Prediction of DNA repair inhibitor response in short-term patient-derived ovarian cancer organoids. *Cancer Discov* **8**, 1404–1421 (2018).
57. Yoshino, Y. et al. Evaluation of site-specific homologous recombination activity of BRCA1 by direct quantitation of gene editing efficiency. *Sci. Rep.* **9**, 1644 (2019).
58. Castroviejo-Bermejo, M. et al. A RAD51 assay feasible in routine tumor samples calls PARP inhibitor response beyond BRCA mutation. *EMBO Mol. Med.* **10**, e9172 (2018).
59. Raevaara, T. E. et al. Functional significance and clinical phenotype of nontruncating mismatch repair variants of MLH1. *Gastroenterology* **129**, 537–549 (2005).
60. Folger, K. R., Thomas, K. & Capecchi, M. R. Nonreciprocal exchanges of information between DNA duplexes coinjected into mammalian cell nuclei. *Mol. Cell. Biol.* **5**, 59–69 (1985).
61. Kucherlapati, R. S., Eves, E. M., Song, K. Y., Morse, B. S. & Smithies, O. Homologous recombination between plasmids in mammalian cells can be enhanced by treatment of input DNA. *Proc. Natl. Acad. Sci. USA* **81**, 3153–3157 (1984).
62. Reeves, R., Gorman, C. M. & Howard, B. Minichromosome assembly of non-integrated plasmid DNA transfected into mammalian cells. *Nucleic Acids Res* **13**, 3599–3615 (1985).
63. Rajendra, E. et al. Quantitative, titratable and high-throughput reporter assays to measure DNA double strand break repair activity in cells. *Nucleic Acids Res* **52**, 1736–1752 (2024).
64. McGivern, A. et al. Promoter hypermethylation frequency and BRAF mutations distinguish hereditary non-polyposis colon cancer from sporadic MSI-H colon cancer. *Fam. Cancer* **3**, 101–107 (2004).
65. Lee, S. Y. Temozolomide resistance in glioblastoma multiforme. *Genes Dis* **3**, 198–210 (2016).
66. Zhu, L. et al. A narrative review of tumor heterogeneity and challenges to tumor drug therapy. *Ann. Transl. Med.* **9**, 1351 (2021).
67. Junttila, M. R. & de Sauvage, F. J. Influence of tumour microenvironment heterogeneity on therapeutic response. *Nature* **501**, 346–354 (2013).
68. Kramer, C. J. et al. RAD51 as a biomarker for homologous recombination deficiency in high-grade serous ovarian carcinoma: robustness and interobserver variability of the RAD51 test. *J. Pathol. Clin. Res.* **9**, 442–448 (2023).
69. Mangogna, A. et al. Homologous recombination deficiency in ovarian cancer: from the biological rationale to current diagnostic approaches. *J. Pers. Med.* **13**, 284 (2023).
70. Cunnea, P. et al. Spatial and temporal intra-tumoral heterogeneity in advanced HGSOC: Implications for surgical and clinical outcomes. *Cell Rep. Med.* **4**, 101055 (2023).
71. Alsaed, B. et al. Intratumor heterogeneity of EGFR expression mediates targeted therapy resistance and formation of drug tolerant microenvironment. *Nat. Commun.* **16**, 28 (2025).
72. FoundationOne CDx technical information. FDA. https://www.accessdata.fda.gov/cdrh_docs/pdf17/P170019B.pdf (2017).
73. MI Cancer Seek technical information. FDA. https://www.accessdata.fda.gov/cdrh_docs/pdf24/P240010B.pdf (2024).
74. Ramón, Y. C. S. et al. Clinical implications of intratumor heterogeneity: challenges and opportunities. *J. Mol. Med.* **98**, 161–177 (2020).
75. Groelly, F. J., Fawkes, M., Dagg, R. A., Blackford, A. N. & Tarsounas, M. Targeting DNA damage response pathways in cancer. *Nat. Rev. Cancer* **23**, 78–94 (2023).
76. Russo, M. et al. Adaptive mutability of colorectal cancers in response to targeted therapies. *Science* **366**, 1473–1480 (2019).
77. Wakimoto, H. et al. Targetable signaling pathway mutations are associated with malignant phenotype in IDH-mutant gliomas. *Clin. Cancer Res.* **20**, 2898–2909 (2014).
78. Wakimoto, H. et al. Maintenance of primary tumor phenotype and genotype in glioblastoma stem cells. *Neuro Oncol* **14**, 132–144 (2012).
79. Wakimoto, H. et al. Human glioblastoma-derived cancer stem cells: establishment of invasive glioma models and treatment with oncolytic herpes simplex virus vectors. *Cancer Res* **69**, 3472–3481 (2009).
80. Cong, L. et al. Multiplex genome engineering using CRISPR/Cas systems. *Science* **339**, 819–823 (2013).
81. Suzuki, T., Ukai, A., Honma, M., Adachi, N. & Nohmi, T. Restoration of mismatch repair functions in human cell line Nalm-6, which has high efficiency for gene targeting. *PLoS One* **8**, e61189 (2013).
82. Kurosawa, A. et al. DNA ligase IV and artemis act cooperatively to suppress homologous recombination in human cells: implications for DNA double-strand break repair. *PLoS One* **8**, e72253 (2013).
83. Saito, S., Kurosawa, A. & Adachi, N. Mechanistic basis for increased human gene targeting by promoterless vectors-roles of homology arms and Rad54 paralogs. *FEBS J* **284**, 2748–2763 (2017).
84. Schrijvers, R. et al. LEDGF/p75-independent HIV-1 replication demonstrates a role for HRP-2 and remains sensitive to inhibition by LEDGINs. *PLoS Pathog* **8**, e1002558 (2012).
85. Iizumi, S. et al. Simple one-week method to construct gene-targeting vectors: application to production of human knockout cell lines. *BioTechniques* **41**, 311–316 (2006).
86. Zhou, J. et al. A first-in-class polymerase theta inhibitor selectively targets homologous-recombination-deficient tumors. *Nat. Cancer* **2**, 598–610 (2021).
87. Kato, S. et al. Precision modeling of gall bladder cancer patients in mice based on orthotopic implantation of organoid-derived tumor buds. *Oncogenesis* **10**, 33 (2021).
88. Matsuura, T. et al. Organoid-based ex vivo reconstitution of Kras-driven pancreatic ductal carcinogenesis. *Carcinogenesis* **41**, 490–501 (2020).
89. Tateishi, K. et al. PI3K/AKT/mTOR pathway alterations promote malignant progression and xenograft formation in oligodendroglial tumors. *Clin. Cancer Res.* **25**, 4375–4387 (2019).
90. Morotomi-Yano, K., Saito, S., Adachi, N. & Yano, K. I. Dynamic behavior of DNA topoisomerase IIβ in response to DNA double-strand breaks. *Sci. Rep.* **8**, 10344 (2018).

91. Kurosawa, A. et al. Arsenic affects homologous recombination and single-strand annealing but not end-joining pathways during DNA double-strand break repair. *FEBS J* **290**, 5313–5321 (2023).
92. So, S., Adachi, N., Lieber, M. R. & Koyama, H. Genetic interactions between BLM and DNA ligase IV in human cells. *J. Biol. Chem.* **279**, 55433–55442 (2004).
93. Fujimaki, K. et al. DNA topoisomerase II inhibitors enhance random integration of transfected vectors into human chromosomes. *Somat. Cell Mol. Genet.* **22**, 279–290 (1996).
94. Yanagibashi, T. I. et al. Complexity of expression of the intermediate filaments of six new human ovarian carcinoma cell lines: new expression of cytokeratin 20. *Br. J. Cancer* **76**, 829–835 (1997).
95. Tomida, J. et al. FAM35A associates with REV7 and modulates DNA damage responses of normal and BRCA1-defective cells. *EMBO J* **37**, e99543 (2018).

Acknowledgements

We thank Takehiko Nohmi and Tetsuya Suzuki for providing us with the pMSH2-Neo plasmid. We thank Etsuko Miyagi and Mae Inada for providing us with the OVSAHO cell line. We thank Promega for their willingness to allow us to modify the *Nluc* gene. We thank Kaoru Okamura, Aya Katsurayama, Akito Oshima, and Yoshiko Hosokawa for excellent technical assistance. This work was supported by JSPS KAKENHI Grant JP19H01151 (N.A.), JSPS KAKENHI Grant JP22K19382 (N.A.), JSPS KAKENHI Grant JP22K09210 (K.T.), JSPS KAKENHI Grant JP24K15289 (S.S.), JSPS KAKENHI Grant JP24K22025 (N.A.), Yokohama City University Strategic Research Promotion Grant SK201901 (N.A.), and the grants for the 2022-2023 and 2024-2025 Research Development Fund and fundraising activities for the YCU Vision 100 Project of Yokohama City University (S.S., S.K., N.A.).

Author contributions

S.S. performed experiments and analyzed the data. N.A. designed the study and analyzed the data. S.K., S.S., N.A., and T.M. conducted the study using ovarian cancer tissues. K.T., S.S., and N.A. conducted the study using brain tumor cells and tissues. U.A. performed drug sensitivity assays and experiments using tumor specimens. A.E. and J.T. contributed to generating *MLH1* mutant cell lines. S.K. and K.T. provided critical advice and reviewed the manuscript. N.A. and S.S. wrote the manuscript. All authors have contributed to the manuscript and approved the manuscript submission.

Competing interests

N.A. is a cofounder and shareholder of DnaQua. All other authors have no competing interests.

Additional information

Supplementary information The online version contains supplementary material available at https://doi.org/10.1038/s41467-025-59462-2.

Correspondence and requests for materials should be addressed to Noritaka Adachi.

Peer review information *Nature Communications* thanks the anonymous reviewers for their contribution to the peer review of this work. A peer review file is available.